https://doi.org/10.5194/egusphere-2026-458
Preprint. Discussion started: 4 February 2026

Impact of Extreme Rainfall on Triggering Conditions and Susceptibility for Shallow landslides: a case study in the Alpes-Maritimes region (France)

Lucie Armand[1,2], Guillaume Chambon[1], Olivier Cerdan[2], Yannick Thiery[3], Nathalie Marçot[4], Louis Ferradou[4], Nicolas Saby[5], Séverine Bernardie[2]

[1]Univ. Grenoble Alpes, INRAE, CNRS, IRD, Grenoble INP, IGE, 38000 Grenoble, France
[2]BRGM, F-45060 Orléans, France
[3]BRGM, F-33600 Pessac, France
[4]BRGM, F-13276 Marseille, France
[5]INRAE, Unité Info&Sol, 45075 Orléans, France

Correspondence to: Lucie Armand (lucie.armand@inrae.fr)

Abstract. Prediction of shallow landslides at the regional scale generally relies on statistical analyses of landslide inventories. Rainfall-duration thresholds and susceptibility maps are among the most common approaches to anticipate future landslide occurrences. However, the outputs and reliability of these approaches can be strongly affected by the representativeness of the landslides included in the inventory. This study specifically investigates the impact of landslides triggered by an extreme rainfall event on the determination of rainfall-duration thresholds and susceptibility maps. We consider the case of Storm Alex, a millennial return period rainfall event, which hit the Alpes-Maritimes region (France) on October 2, 2020. The analysis is based on an inventory of 5,383 shallow landslides, including 1,656 landslides triggered by Storm Alex. The CTRL-T algorithm was used to compute statistical rainfall-duration thresholds with and without the inclusion of Storm Alex landslides. A Random Forest approach was used to produce and compare susceptibility maps under the same two configurations. Results show that: (a) rainfall-duration thresholds derived from datasets including Storm Alex landslides are significantly higher; (b) the exceptional rainfall intensity triggered landslides in areas having an initial lower susceptibility; and (c) including these events in susceptibility modeling alters the spatial distribution of susceptibility values. This study provides a quantitative analysis of the impact of landslides triggered by extreme rainfall events on statistical prediction models.

1 Introduction

Mountainous areas are highly prone to mass wasting processes, among which shallow landslides, also called soil slip (Cruden and Varnes, 1996) are frequently observed. In this study, a shallow landslide is defined by a sudden and relatively rapid movement of the material overlying the bedrock, typically involving a 1–2 m thick soil layer. These phenomena can cause significant damage to infrastructures and, in some cases, endanger human lives. They also play a role in the natural

https://doi.org/10.5194/egusphere-2026-458
Preprint. Discussion started: 4 February 2026

evolution of slopes, by reshaping the landscapes and participating in sediment transfer (Clapuyt et al., 2019). Thus, improving knowledge on landslide triggering conditions is essential for a reliable risk assessment, land use planning strategies and the establishment of effective early warning systems.

Rainfall plays a major role in triggering shallow landslides (Iverson, 2000), since intense or prolonged precipitation events can rapidly increase soil moisture and pore water pressure, decreasing slope stability (Montrasio and Valentino, 2008; Tsai, 2008). The first attempts at linking rainfall to landslide occurrence were based on simple empirical thresholds, such as those introduced by Caine (1980) and later by (Terlien, 1998). Based on these pioneer studies, various empirical, statistical and probabilistic approaches were developed to better identify the rainfall conditions favourable to landslides. Among these different approaches, cumulative/duration thresholds (ED thresholds), which combine the cumulative precipitation and the duration of rainfall events associated with landslides, have taken an important place (Segoni et al., 2018). They provide a simple and robust tool, used in several regions of the world to design early warning systems (Segoni et al., 2018; Gonzalez et al., 2024).

Susceptibility maps are another key tool in the analysis of landslide processes. Susceptibility represents the likelihood of landslide occurrence at any given location, regardless of the temporal probability (Fell et al., 2008; Corominas et al., 2014). In our case, susceptibility maps aim to identify areas prone to shallow landslides based on terrain characteristics. They are based on the combination of various predisposing factors, the most common of which include geomorphological features (e.g. slope, aspect, curvature, landform), geological features (e.g. lithology, distance to fault), or soil properties (e.g. soil thickness, texture) (Reichenbach et al., 2018). The construction of susceptibility maps can be based on deterministic methods (i.e. simulating slope stability using physical parameters) (Gökceoglu and Aksoy, 1996; Armaş et al., 2014; Pradhan and Kim, 2016), or on statistical and machine learning approaches (Reichenbach et al., 2018). Among these, Random Forest (RF) has become increasingly popular in recent years, due to its robustness and high predictive capabilities (Trigila et al., 2015; Chen et al., 2017; Park and Kim, 2019), and has been largely applied to compute susceptibility maps (Catani et al., 2013; Reichenbach et al., 2018; Taalab et al., 2018; Sun et al., 2020; Zhou et al., 2021).

These tools, rainfall thresholds and susceptibility maps, are usually established using inventories of past landslides. The assumption here is that knowledge of past events is valuable to guide the prediction of future instabilities. This requires representative inventories including landslides triggered by different rainfall intensity, ranging from moderate to extreme rainfall events. However, extreme rainfall typically triggers a large number of landslides. Rainfall intensity strongly affects soil infiltration patterns and hydrological response (Iverson, 2000; Ran et al., 2018), which can modify the triggering mechanisms of landslides compared to more moderate rainfall events. Recent studies have shown that, during years characterized by extreme rainfall, certain morphological factors, such as slope, local relief, and excess topography, become more determinant in controlling landslide occurrence (Jones et al., 2021). This indicates that landslides triggered by extreme rainfall do not necessarily follow the same spatial patterns as more common events, which highlights the importance of examining their impact on predictive models. However, this topic is currently poorly documented in the literature.

https://doi.org/10.5194/egusphere-2026-458
Preprint. Discussion started: 4 February 2026

A few studies focus on the effect of extreme rainfall on slope stability (Shou and Lin, 2020), on forecasting landslides triggered by such rainfall (Lee et al., 2008; Lombardo et al., 2014), or on how extreme rainfalls may alter the slopes susceptibility in the long term (Bebi et al., 2019; Jones et al., 2021; Achu et al., 2024). In this study, we are interested in examining the specificities of landslides triggered by extreme rainfall events in terms of predisposing factors, and in quantifying their influence on the robustness of susceptibility maps and ED rainfall thresholds. The general hypothesis behind this question is that landslides triggered by an extreme rainfall event exhibit specific triggering conditions and predisposing patterns that can alter the generalization capacity of predictive models. Storm Alex, which occurred on October 2, 2020 in the Alpes-Maritimes region (France) and is estimated to have had a millennial return period, is used as a representative case study for an extreme rainfall event. The analysis of cumulative rainfall/duration thresholds makes it possible to assess how the inclusion of Storm Alex landslides in the inventory modifies the statistical triggering conditions. Susceptibility maps allow us to quantify the impact of landslides triggered by an extreme rainfall event on the spatial distribution of areas prone to landslides. Analysing these effects can help to better understand the limits of data-driven models and could help to understand how to calibrate tools used for anticipating landslides in meteorological contexts prone to extreme rainfall events.

This article begins with an overview of the study area and the description of the Storm Alex extreme rainfall event (Sect. 2). It is followed by a detailed presentation of the datasets used, including meteorological information, predisposing factors and the landslide inventory (Sect. 3). The methodological framework is then described, focusing on the computation of rainfall-duration thresholds using the CTRL-T algorithm and the development of susceptibility maps based on Random Forest algorithm (Sect. 4). The subsequent section presents and compares the results obtained for both the thresholds and susceptibility maps (Sect. 5). Finally, the discussion highlights the main insights derived from the analysis (Sect. 6), before the conclusion summarizes the key contribution, limitations, and future research (Sect. 7).

2 Context

2.1 Study area

The Alpes-Maritimes region is located in the southeastern part of France, bordering the Mediterranean Sea (Fig. 1a). Spanning an area of 1,299 km², this region has a population of 1.1 million inhabitants (INSEE, 2022), of which 94% are concentrated in the 66 municipalities surrounding the Mediterranean coast. It presents a contrasting geomorphological context, with the northern part dominated by high mountainous relief and deep valleys shaped by glaciers, while the southern part exhibits gentler terrain and pronounced urbanization along the coast. The elevation varies from sea level to 3,143 m.

The harmonized geological map of the Alpes-Maritimes (Gonzales, 2008) indicates that the territory exhibits a highly diverse geology, with a majority (77%) of sedimentary rocks (Fig. 1b). Marly and clayey formations weather into clay-rich soils that are highly sensitive to water saturation and alteration. In addition, recent unconsolidated deposits such as moraines

https://doi.org/10.5194/egusphere-2026-458
Preprint. Discussion started: 4 February 2026

(3%), alluvial deposits (5%) and scree or debris cone deposits (20%), represent unstable materials that can further increase the susceptibility to landslides.

The study area presents four main types of climates (Joly et al., 2010), including Mediterranean climate, altered Mediterranean climate, semi-continental climate, and mountain climate (Fig. 1c). This climatic heterogeneity implies differences in precipitation regimes, as shown in Fig.1d, which represents the mean annual rainfall over the period 1997-2019. Mountainous areas typically receive more precipitation (from 1000mm.yr-1 to more than 1300mm.yr-1) than Mediterranean areas (< 900mm.yr-1). However, the latter are characterized by a pronounced seasonal regime (Fig. 3c), with a cold season marked by a higher amount of rainfall (Lionello et al., 2006), and a dry season favourable to intense and localized rainstorms that can generate landslides as well as other geomorphological processes (torrential floods, debris flows, rockfalls…etc) (Rebora et al., 2013; Liébault et al., 2024).

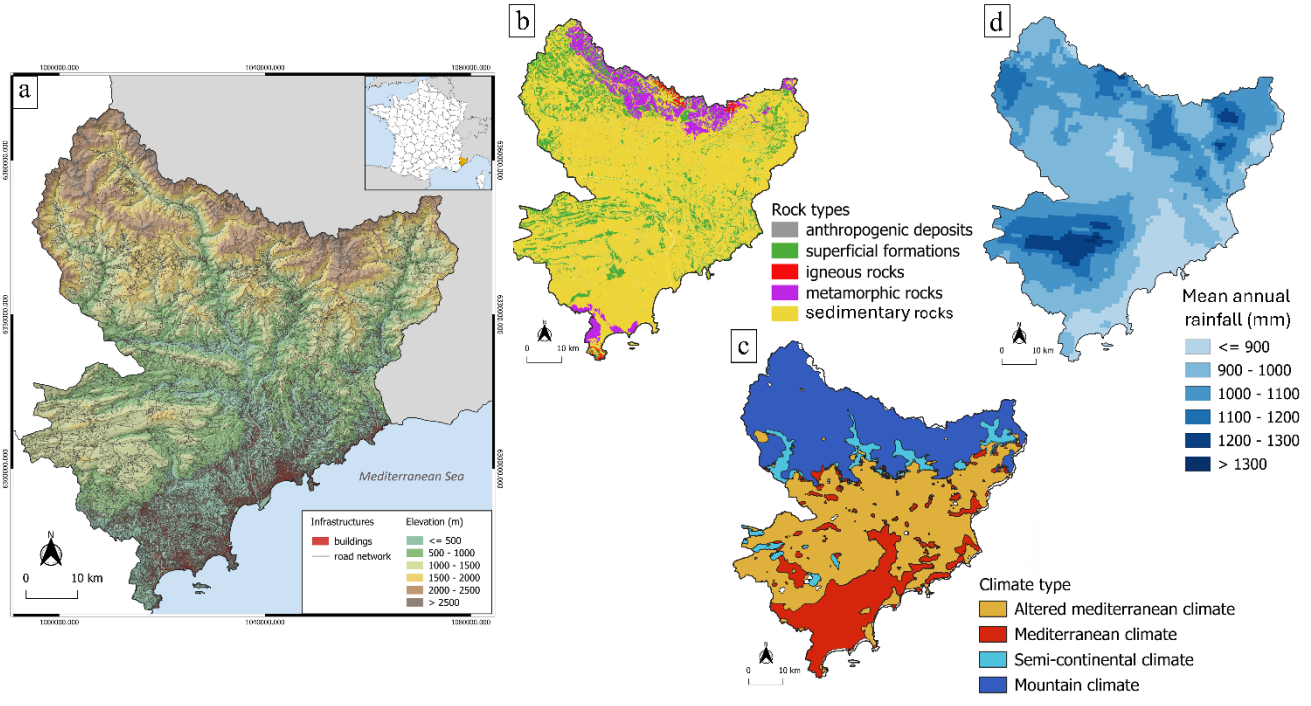

Figure 1: (a) Overview of the study area. (b) Main rock types. (c) Climatic classification according to Joly et al. (2010). (d) Spatial distribution of the mean annual rainfall over the period 1997-2019 (COMEPHORE radar data).

2.2 Storm Alex

On October 2, 2020, a large part of the Alpes Maritimes region was affected by Storm Alex, an extreme rainfall event with a millennial return period (Carrega and Michelot, 2021). These record-breaking rainfalls were caused by a combination of meteorological conditions favourable to stationary thunderstorms, enhanced by the mountainous terrain and a significant influx of moisture from the Mediterranean area (Chochon et al., 2022). The valleys of Tinée, Vésubie and Roya were

https://doi.org/10.5194/egusphere-2026-458
Preprint. Discussion started: 4 February 2026

particularly impacted by the storm (Fig. 2a). For example, the municipality of Tournefort recorded 600 mm in 24 hours (Fig. 2b). The rainfall began on October 2 at 01:00 am and lasted until the end of the same day. This exceptional rainfall event deeply altered the landscape and triggered violent floods as well as numerous mass movements, including shallow landslides, debris flows, and bank erosion. The storm is responsible for the death of 17 people, and hundreds of people were evacuated. The event caused significant damage to infrastructure, with an estimated cost exceeding 1 billion euros (Arbizzi et al., 2021).

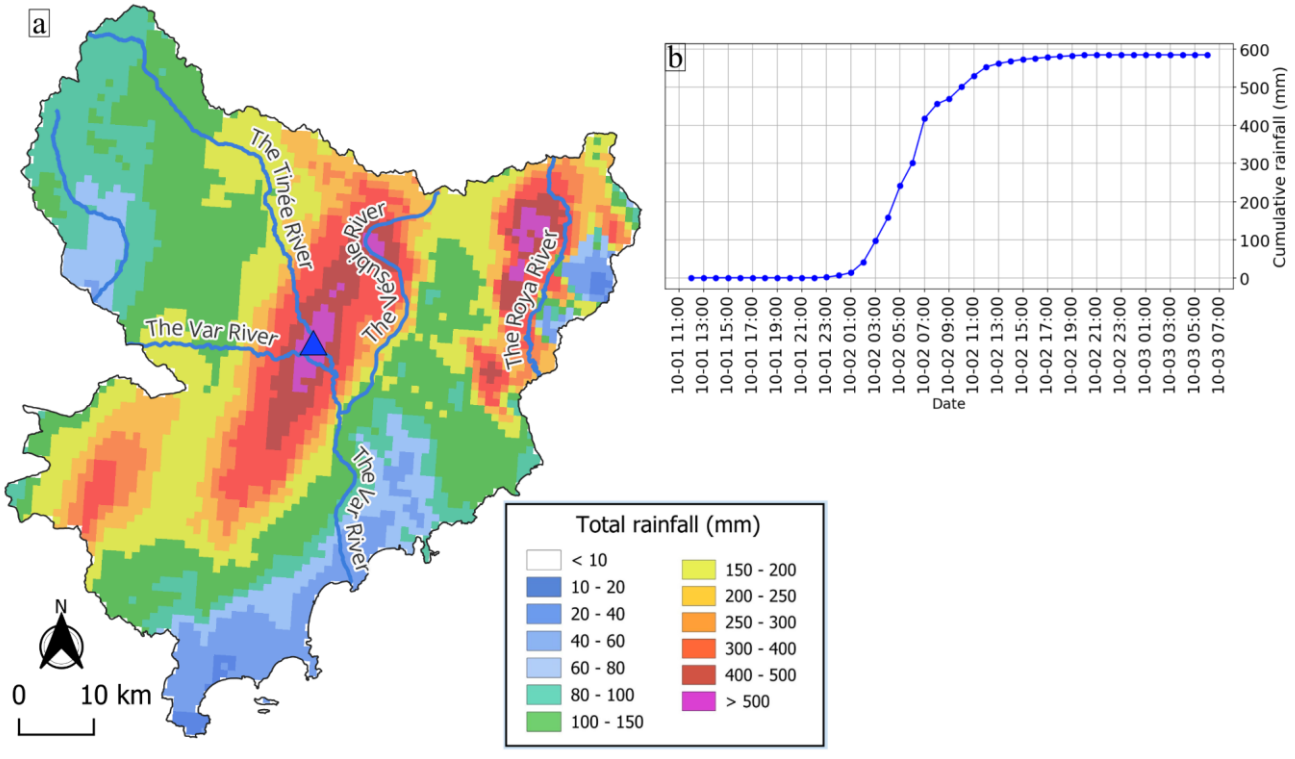

Figure 2: Spatio-temporal description of Storm Alex. (a) Map of recorded rainfall accumulation during Storm Alex, from October 1, 2020, at 12:00 PM to October 3, 2020, at 06:00 AM (COMEPHORE data, Météo-France). The blue triangle represents the location of Tournefort municipality. (b) Accumulated rainfall over Tournefort municipality

3 Data

3.1 Meteorological data

Two meteorological datasets have been exploited for the computation of ED rainfall thresholds. Precipitation data derived from the COMEPHORE dataset are used to characterize rainfall events. COMEPHORE is a meteorological product provided by Meteo-France, covering the metropolitan French territory (Tabary et al., 2012). It consists of hourly accumulated

https://doi.org/10.5194/egusphere-2026-458
Preprint. Discussion started: 4 February 2026

precipitation on a spatial grid of 1 km × 1 km, resulting from the fusion of radar measurements and in situ observations from a rain gauge network. The data are available from 1997-01-01 to the present day.

The second used dataset, SIM (SAFRAN-ISBA-MODCOU), is a hydrometeorological reanalysis. It results from the combination of a meteorological model (SAFRAN), a land surface model (ISBA), and a hydrogeological model (MODCOU) (Habets et al., 2008). The dataset, also distributed by Météo-France, provides 25 climatic and hydrological variables at a daily time step and on a regular grid of 8 km × 8 km. In this study, we used the temperature and potential and real evapotranspiration. Data are available from 1958-08-02 to the present day.

3.2 Predisposing factors

Eleven predisposing factors were analysed, including geologic, topographic, and soil properties, all in raster format (see Fig. A1**):**

- *Lithology* is obtained from the harmonized geological map of the Alpes-Maritimes region at 1:50,000 scale (Gonzales, 2008). The 274 initial classes were grouped into 28 classes (Fig. A1a) based on prior knowledge about susceptibility of lithologies to landslides.
- *Land cover* data come from the CORINE Land Cover Level 2 (2006 edition), a satellite-derived European product comprising 13 classes, with a spatial resolution of 25 meters (Fig. A1b).
- A 25m DEM provided by the French National Institute of Geographic and Forest Information (https://www.data.gouv.fr/datasets/bd-alti-r-1/) was used to derive *slope* (Fig. A1c), *Topographic Positional Index (TPI)* (Fig. A1d), and *aspect* (Fig. A1e) using GDAL tools and a 3x3 pixel window in QGIS software.
- *Landform (Iwahashi and Pike)* (Iwahashi and Pike, 2007) was derived from the DEM using the SAGA *Terrain Surface Classification* tool in QGIS, with 8 classes, a four-neighbour Laplacian Filter, and a 10 pixels window (Fig. A1f).
- *Landform (Weiss)* (Weiss, 2001) was derived from the DEM using the *TPI Based Landform Classification* tool, and a bandwidth equal to 400 m, resulting in 10 classes (Fig. A1g). Note that, although the Weiss landform classification is derived from TPI values, the two metrics are complementary. TPI indicates the relative elevation of a given pixel, compared to neighboring pixels, thus capturing fine-scale variations. The Weiss landform integrates TPI at a larger scale, defined by the bandwidth parameter, to produce a categorical classification of larger-scale morphological patterns.
- *The general curvature* (Fig. A1h) was also calculated from the DEM using the SAGA toolbox, applying the 9 parameters second-order polynomial method (Zevenbergen and Thorne, 1987).
- Three rasters of soil texture, namely the percentages of *clay* (Fig. A1i), *sand* (Fig. A1j), and *silt* (Fig. A1k) in the upper 30 cm of soil, were used. These three products are available at national scale with a 90 meters spatial resolution. They are obtained from a Random Forest algorithm calibrated with French soil samples from the 0-30 cm topsoil layer and using a set of environmental covariates such as terrain, climate, vegetation, geology, land use and satellite indices (Suleymanov et al., 2024).

https://doi.org/10.5194/egusphere-2026-458
Preprint. Discussion started: 4 February 2026

The eleven rasters of predisposing factors were harmonized onto a common 25 m resolution grid using QGIS resampling tool, with the DEM as the reference.

3.3 Landslide inventory

3.3.1 General description

The landslide inventory used in this study relies on previous mapping efforts (Lucas, 2023; Thiery et al., 2025). It comprises 5,383 rainfall-induced shallow landslides distributed across the study area (Fig. 3a). This inventory covers a period of nearly 330 years, ranging from 1696 to 2024 (Fig. 3b). The monthly distribution (based on 2,645 landslides) reveals a seasonal trend in landslide occurrence, with the highest number of events recorded during the cold season (from October to January). This trend closely matches the mean monthly rainfall (Fig. 3c).

In the inventory, 28.3% of the landslides were taken from pre-existing databases, including those of the RTM service (https://geo-onf.opendata.arcgis.com/maps/760c436f2736431fb0cae21c14c7414b/about), of the French Geological Survey (https://www.georisques.gouv.fr/donnees/bases-de-donnees/base-de-donnees-mouvements-de-terrain), of the CEREMA, of the municipality of Menton, of the Departmental Council of Alpes Maritimes, and of the Regional Observatory for Major Risks (ORRM). In addition, numerous landslides were added through diachronic analysis of orthophotographs controlled by field recognitions (69.3%), and oral testimonies (2.4%). To ensure data quality and reliability, the inventory was rigorously checked to remove duplicates from different sources, non-superficial landslides, and anthropogenic landslides.

Landslides in the database were initially represented either as polygons (75.8%) or points (24.2%). Among the polygons, 61.5% include an accurate delineation of the ablation zone (Lucas, 2023). To create a homogeneous database, all polygons were converted into points, using either the centroid of the entire polygon or, when available, the centroid of the ablation zone. The location of each landslide was verified using textual information from the database when available, further improving the spatial accuracy of the dataset (Fig. 3d). A landslide is described as decametric when its location is estimated with meter-scale accuracy, hectometric when the accuracy is on the order of 100 meters, and kilometric when the location is known only at the kilometer scale. The temporal accuracy of the landslides is also indicated in Fig. 3d. All the landslides with *unknown* temporal accuracy correspond to those reported from orthophotographs.

The shallow landslides of the inventory are categorized into five distinct types, based on textual information and orthophotographs. Cut-slope landslides (13.9%) develop where the basal part of a slope has been artificially excavated, resulting in destabilization. This type of landslide is predominantly located along the road network. Riverbank landslides (9.7%) are triggered by lateral river erosion, which induces basal undercutting of the bank. This undercutting destabilizes the lower part of the slope and can lead to a landslide propagating upslope, especially during flood events. Midslope landslides (41.3%) occur in the middle of slopes, in areas unaffected by artificial excavations or riverbank erosion. Lastly, flow-like landslides (34.1%) are characterized by long-distance propagation. The remaining landslides (1.0%) have an unknown type

https://doi.org/10.5194/egusphere-2026-458
Preprint. Discussion started: 4 February 2026

due to lack of textual information and poor spatial accuracy. Note that all riverbank landslides were systematically excluded from further analysis, as their triggering is primarily governed by erosion rather than rainfall itself.

Among the 5,383 landslides, 1,655 were directly associated with Storm Alex (Thiery et al., 2025). In the absence of precise information regarding the time of occurrence of the Ales-induced landslides, they have all been dated on 3 October, i.e. the day after the storm. They are mostly concentrated in the Vésubie, Tinée, and Roya valleys, due to two main causes: first, the strongest impact of the storm was located in these valleys (Fig. 2); and second, most Alex-induced landslides were identified through an orthophotograph acquired shortly after the storm, which was available only for these three valleys (post-Alex ortho-express, delimitation shown in Fig. 3a). Note that some landslides detected using the 2023 orthophotographs but outside of the ortho-express coverage could also have been triggered by the storm. However, due to lack of accurate dating, these landslides have not been associated with the Storm Alex.

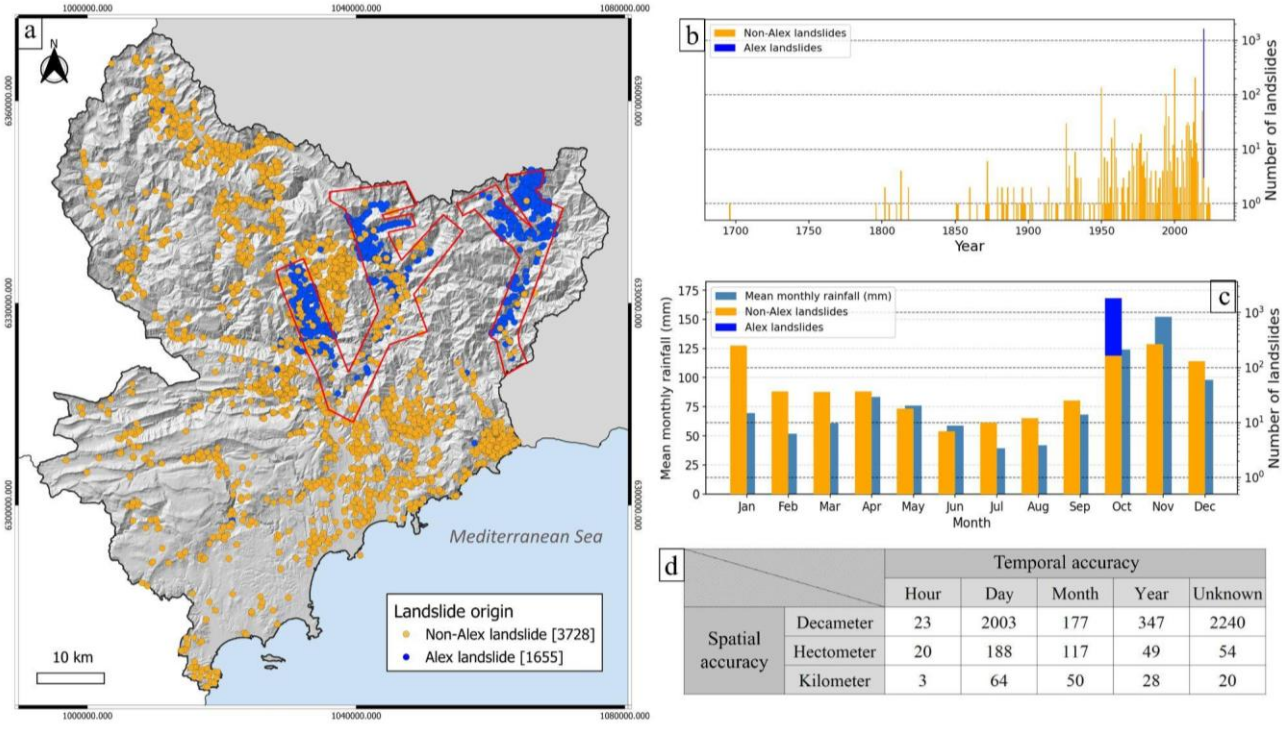

d

		Temporal accuracy				
		Hour	Day	Month	Year	Unknown
Spatial accuracy	Decameter	23	2003	177	347	2240
	Hectometer	20	188	117	49	54
	Kilometer	3	64	50	28	20

Figure 3: Spatio-temporal characterization of the landslide inventory across the study area. (a) Spatial distribution of Alex (blue), and non-Alex (orange) landslides. Red outlines indicate the area covered by the post-Alex ortho-express. (b) Yearly distribution of the landslides. (c) Monthly distribution of the landslides and mean monthly cumulative rainfall over the study area. (d) Spatial and temporal accuracy of the landslides.

3.3.2 Subsets used for rainfall thresholds and susceptibility analysis

Three different subsets were extracted from the global inventory to carry out the different analyses. The subset used for the ED rainfall threshold analysis includes 1,746 landslides with daily accuracy to ensure reliable comparison with the meteorological data, and decametric to hectometric spatial accuracy suitable for matching with the 1×1 km resolution of the

https://doi.org/10.5194/egusphere-2026-458
Preprint. Discussion started: 4 February 2026

rainfall data grid. Only landslides dated after January 1, 1997 were considered, as meteorological data are only available after this date. In this subset, 1,335 landslides are associated with Storm Alex (Fig. 4a).

For the analysis of susceptibility only landslides with decametric spatial accuracy were retained. For comparing the distributions of predisposing factors between Alex and non-Alex landslides, the selection was further restricted to landslides located within the area covered by the post-Alex ortho-express to avoid any bias. For both subsets, a small number of landslides (66 and 11, respectively) occurred on slopes less than 10°. These landslides were excluded, as their location was considered likely erroneous. The final subsets consist of 4,200 landslides for the susceptibility assessment (of which 1,319 were induced by Storm Alex) and 1,544 landslides for the distribution analysis (of which 1,263 were induced by Storm Alex) (Fig. 4b-c).

For clarity, Storm Alex-induced landslides are hereafter denoted Alex landslides, whereas non–Storm Alex-induced landslides are denoted non-Alex landslides. In every subset, datasets including Alex landslides are designated as WSAL (*With Storm Alex Landslides*), and those excluding Alex landslides are designated as WoSAL (*Without Storm Alex Landslides*).

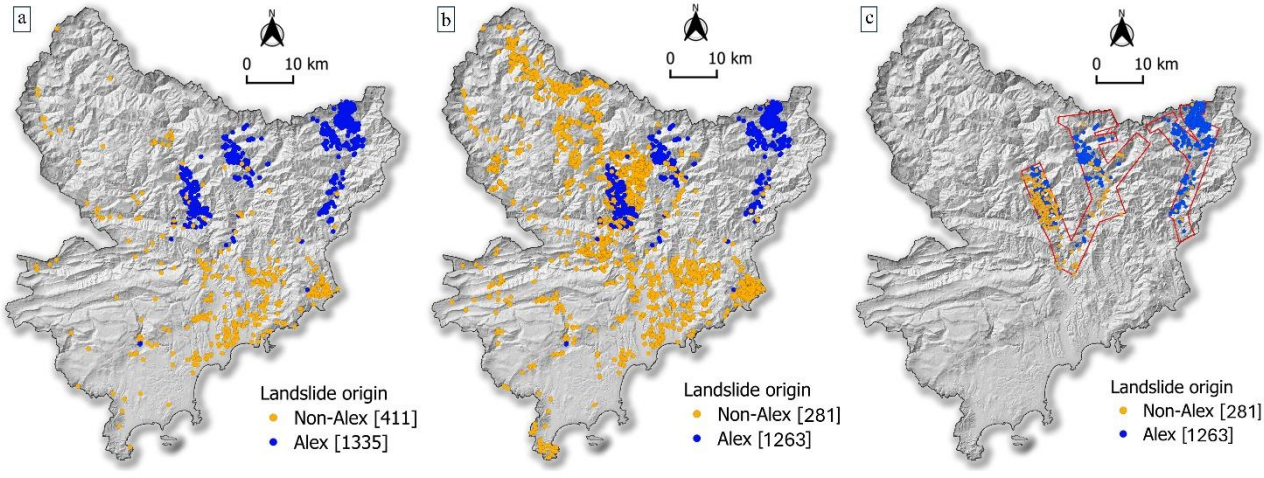

Figure 4: Spatial distributions of landslides subsets used for the analyses. (a) Landslides used for ED rainfall threshold analysis; (b) Landslides used for susceptibility analysis; (c) Landslides used for comparing the distributions of predisposing factors. Blue points represent Alex landslides and orange points represent non-Alex landslides.

4 Methods

As explained in the introduction, the main objective of this study is to compare rainfall thresholds and susceptibility maps constructed with and without the landslides triggered by Storm Alex. Cumulative/duration (ED) thresholds are computed based on COMEPHORE rainfall data. Landslide susceptibility is assessed using a Random Forest (RF) algorithm with the eleven predisposing factors described in Sect. 3.2.

https://doi.org/10.5194/egusphere-2026-458
Preprint. Discussion started: 4 February 2026

4.1 ED rainfall thresholds

The ED thresholds were computed using the CTRL-T algorithm (Calculation of Thresholds for Rainfall-Induced Landslides; Melillo et al., 2015, 2018). This tool is based on a frequentist approach, allowing the definition of thresholds for a specified non-exceedance probability Required input data are precipitation time series and a well-dated landslide inventory.

The algorithm is divided into three blocks. For each grid point of the COMEPHORE rainfall dataset, the first block segments raw precipitation data into rainfall events and sub-events, defined as periods of continuous precipitation bounded by dry periods of a minimum duration. In the warm season, the minimum duration for these dry periods is 48 and 6 hours for rainfall events and sub-events, respectively. In the cold season, these minimum durations are multiplied by a spatially-varying factor ranging from 1 to 3. This factor accounts for the climatic heterogeneity within the study area. It is computed from SIM climatic parameters according to Barthélemy et al. (2024).

In the second block, the time of occurrence of each landslide in the inventory is compared to rainfall events and sub-events of all COMEPHORE grid points located within a 1,000 m radius around the landslide location. For daily-dated landslides, the hour of occurrence is arbitrarily fixed at 12:00 pm. The MRC (Multiple Rainfall Conditions) dataset is built by aggregating, for each landslide, all the possible combinations of event duration (D) and cumulative rainfall (E) in the 1,000 m radius (including both rainfall events and sub-events). Next, each (D,E) pair of the MRC dataset is weighted according to the values of D and E, and to the distance between the grid point and the landslide. The algorithm selects, for each landslide, the (D,E) pair with the highest weight to create the MPRC (Most Probable Rainfall Conditions) dataset.

Finally, the last block computes thresholds for both MRC and MPRC datasets, using a frequentist method (Brunetti et al., 2010) combined with a bootstrapping (Peruccacci et al., 2012) with 100 repetitions to assess uncertainties. The thresholds assume the equation defined in Eq. (1):

$$E = (\alpha \pm \Delta\alpha) \times D^{(\gamma \pm \Delta\gamma)} \qquad (1)$$

with E the cumulative rainfall (in mm) of the rainfall event, D its duration (in h), α a scaling parameter and γ the shape parameter. $\Delta\alpha$ and $\Delta\gamma$ represent the uncertainties on α and γ, respectively.

In this study, thresholds corresponding to a 5% non-exceedance probability were computed, following the approach adopted in previous studies (Marra, 2019; Peres and Cancelliere, 2021). Only thresholds derived from the MPRC datasets are considered in the following.

4.2 Susceptibility assessment

Assessing landslide susceptibility requires accounting for complex interactions between topographic and geomorphological factors. In this study, a Random Forest (RF) method (Breiman, 2001) was selected for its robustness and its ability to capture nonlinear relationships between diverse variables (called *features*), while maintaining high predictive accuracy (Chen et al.,

https://doi.org/10.5194/egusphere-2026-458
Preprint. Discussion started: 4 February 2026

2017; Ng et al., 2021; Trigila et al., 2015). RF is generally less prone to overfitting than other machine learning algorithms (Breiman, 2001). Overfitting happens when a model is too closely adapted to the training data, and performs poorly on new data. It also allows the assessment of features importance, which in our case can provide useful insight into the main factors controlling landslide occurrence. The suitability of RF for spatial analyses of landslide susceptibility is reflected in its widespread application in previous research (Catani et al., 2013; Taalab et al., 2018; Sun et al., 2020; Li et al., 2022; Nocentini et al., 2024).

4.2.1 Random Forest algorithm

RF is a supervised learning algorithm, based on the bagging (Bootstrap Aggregating) principle: multiple independent decision trees are created and their predictions are combined to indicate a final result. Each tree is built by randomly selecting subsets of features (i.e., the predisposing factors in our case) and observations (i.e., the landslides and non-landslides). At each division point (node) of a tree, the algorithm chooses the best split among these subsets to separate the data. This double random selection increases the diversity of trees and reduces overfitting.

Here, the output of each tree is the occurrence or not of a landslide. For a classification problem, the final prediction corresponds to the majority class predicted by all the trees. In this study, the proportion of trees that predicted the positive class (i.e. landslide occurrence) is considered as a susceptibility score. It is important to realize that this score does not represent absolute probability of landslide occurrence. It should rather be regarded as a relative index of similarity between the predisposing factors at a given pixel on the map and those observed for landslides in the inventory.

4.2.2 Non-landslides sampling

In the context of supervised landslide susceptibility modeling, providing non-landslide samples is a crucial step that can strongly influence model performance and final results (Fu et al., 2025). The objective is to prevent the model from being biased towards the positive class (i.e. landslides). However, the selection of non-landslide locations involves a degree of arbitrariness. A common approach is to generate non-landslide points outside a buffer zone around known landslides (Gu et al., 2024, 2023). Following this approach, and considering also that landslides occurring near major infrastructures are more likely to be reported, we defined a valid area for non-landslide sampling as a 1 km buffer around major roads and excluding areas located within a 150 m radius from recorded landslides (Fig. A2).

To account for the variability related to the location of non-landslide points, 50 distinct datasets were generated for each scenario (i.e., with and without Alex landslides), keeping landslide points fixed while randomly generating non-landslide points within the valid area. A balanced 1:1 ratio between landslide and non-landslide points was maintained to prevent class imbalance. Non-landslides points were first generated in the valid area for the WSAL datasets (i.e including Alex landslides). Each of these 50 datasets therefore include 4,200 landslides points and 4,200 non-landslides points. To generate the corresponding 50 WoSAL datasets (i.e. excluding Alex landslides), we started from the 50 WSAL datasets. In each dataset, the 1,319 Alex landslides were removed. Then, in each dataset, an equal number of non-landslide points was

https://doi.org/10.5194/egusphere-2026-458
Preprint. Discussion started: 4 February 2026

randomly excluded. This approach avoids regenerating non-landslide points for the WoSAL datasets, which could potentially result in non-landslide points where Alex landslides had occurred. It also minimizes the differences in the spatial distribution of non-landslide points between the WSAL and WoSAL datasets, ensuring that subsequent analyses are not biased by variations in non-landslide locations. The procedure to generate the datasets is summarized on Fig. 5.

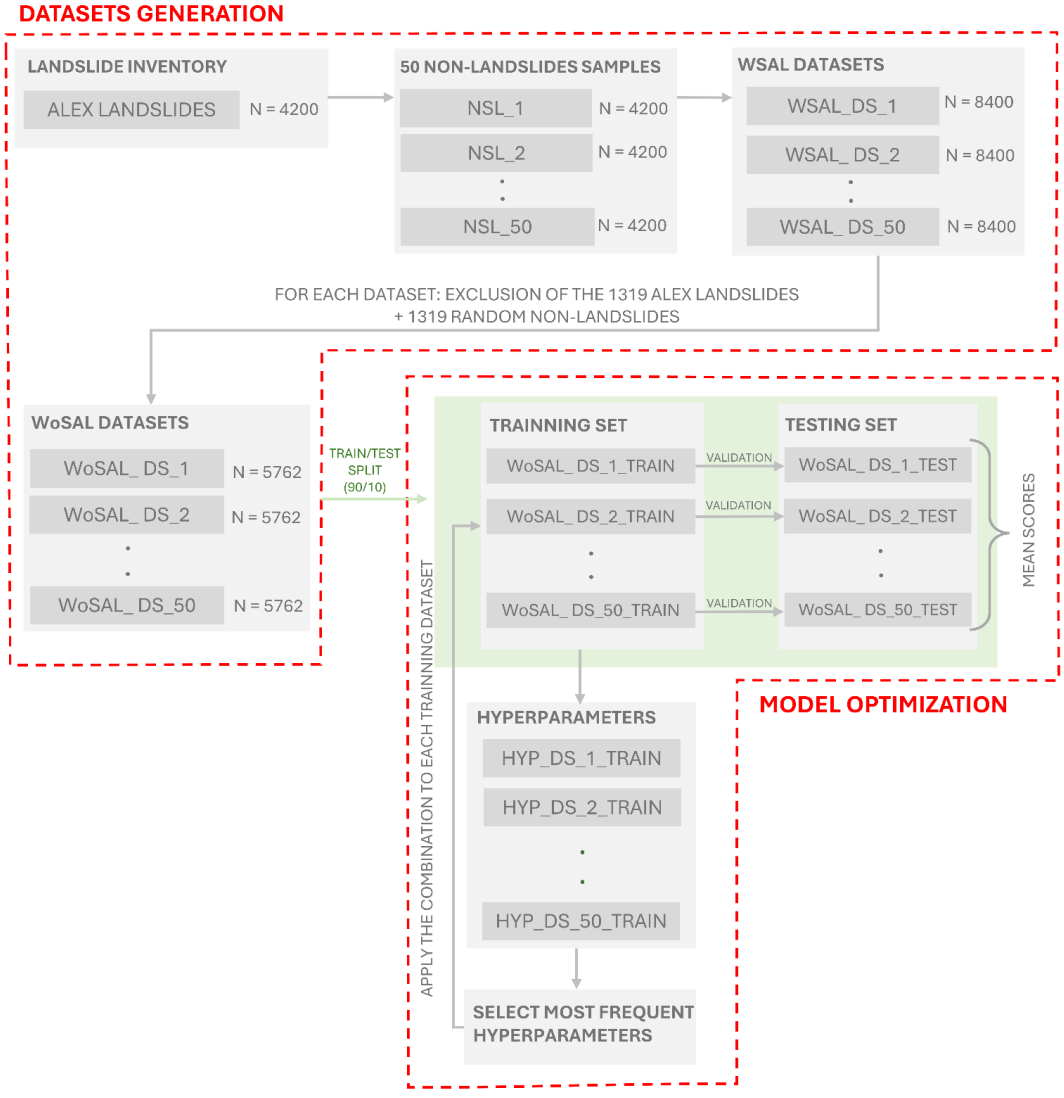

Figure 5: Workflow of datasets generation and model optimization procedures.

4.2.3 Model optimization

Categorical features (lithology, landcover, and both landforms) were encoded using a One Hot Encoder. Hyperparameter optimization was performed on the WoSAL datasets using exhaustive GridSearch with five-fold cross-validation

https://doi.org/10.5194/egusphere-2026-458
Preprint. Discussion started: 4 February 2026

(GridSearchCV) on 90% of each of the 50 datasets. These 90% training sets were constructed so that landslide points remained identical across all datasets, and each set maintained a balanced 1:1 ratio of landslide to non-landslide points.

The GridSearchCV procedure explores a predefined grid of hyperparameters, summarized in Table 1, and retains the combination with the highest average accuracy score over the five folds. For each of the 50 datasets, an independent GridSearchCV was conducted, leading to 50 distinct optimal combinations. The most frequently selected combination was then applied to each training dataset to fit the model, which was subsequently validated on the corresponding 10% validation set. The final selected combination, which was selected 27 times, is indicated in Table 1. The workflow of model optimization is presented on Fig 5. The mean performance scores over the 50 datasets, including accuracy, area under the ROC curve (AUC-ROC), F1 score, and recall, with their corresponding standard deviations, minimum and maximum values are presented in Table 2. Overall, the results indicate that the model performs well across all datasets.

Hyperparameter	Description	Tested values
n_estimator	Number of trees in the model	200, 500, **800**
max_depth	Maximum depth of each tree	**None**, 10, 20
min_samples_split	Minimum number of samples required to split an internal node	**2**, 5, 10
min_samples_leaf	Minimum number of samples required to be at a leaf node	**1**, 5, 10
max_leaf_nodes	Maximum number of terminal (leaf) nodes in a tree	**None**, 100, 300

Table 1: Hyperparameter tested during GridSearchCV. Bold values indicate the ones that were selected.

Score	Mean	Standard deviation	Min	Max
Accuracy	0.81	0.01	0.77	0.84
AUC-ROC	0.90	0.01	0.88	0.92
F1 Score	0.81	0.01	0.78	0.84
Recall	0.83	0.01	0.81	0.85

Table 2: Mean performance metrics of the model across the 50 datasets, including accuracy, AUC-ROC, F1 score, and recall, along with their standard deviations, minimum and maximum values

https://doi.org/10.5194/egusphere-2026-458
Preprint. Discussion started: 4 February 2026

4.2.4 Mean susceptibility maps

Once the optimal combination of hyperparameters is identified and validated, a Random Forest was retrained on each complete dataset, in order to fully exploit all available information. This step was carried out on the 50 datasets for each scenario. For every trained model, a susceptibility map was generated. The susceptibility values assigned to each pixel correspond to the proportion of trees predicting a landslide occurrence. To integrate the variability related to the random selection of non-landslides points, the final map for each scenario is calculated as the average of the 50 individual maps. We checked that 50 non-landslides scenarios are sufficient to obtain a converged standard deviation among the individual maps. The spatial resolution of the final susceptibility maps is 25 m, i.e., the same as the rasters of predisposing factors.

4.2.5 Permutation importances

Permutation importance is used to assess the relative influence of each feature on the predictions of the model. The principle consists in measuring the performance decrease when the values of a given feature are randomly shuffled. In practice, the accuracy of the model is first calculated on a test set (Altmann et al., 2010). The values of a given feature are then shuffled in the test set and the accuracy is recalculated. This process is repeated for all the features, once at a time. A larger decrease in accuracy indicates that the feature is more important for predictions. In this study, the use of One Hot encoding generated many binary variables from the same categorical feature, making it difficult to interpret the importance of individual features. To address this issue, a grouped permutation importance was applied, where all variables derived from the same original feature are permuted simultaneously. For the importance analysis, each dataset was split into 80% training and 20% test sets. This procedure was performed for all 50 datasets in both the WSAL and WoSAL datasets. For each split, the permutation importance of each feature group was calculated over 20 repetitions, and the reported importance values correspond to the averages across these 20 repetitions and the 50 datasets.

5 Results

5.1 ED thresholds

The ED rainfall thresholds derived from the MPRCs (Most Probable Rainfall Conditions) are presented in Fig. 6. Both thresholds represent the 5% non-exceedance probability: the black threshold is based on the WSAL dataset, while the grey threshold is based on the WoSAL dataset. The associated uncertainties, estimated through the bootstrapping approach, are shown in light grey.

Each point on the plot represents an individual landslide, with orange points corresponding to non-Alex landslides and blue points representing Alex landslides. All of the 1,335 Alex landslides could be associated with a rainfall event, except for two that occurred on October 7 and 8 (hence several days after the storm), for which no rainfall was recorded. Among the 411 non-Alex landslides initially present in the subset, only 371 were used for the threshold computation. The 40 excluded

https://doi.org/10.5194/egusphere-2026-458
Preprint. Discussion started: 4 February 2026

landslides were omitted either because they occurred more than 48 hours after the end of the reconstructed rainfall event or because the cumulative rainfall was less than 5 mm. These exclusion criteria are directly implemented in the CTRL-T algorithm.

Non-Alex landslides are widely distributed, with rainfall durations ranging from 44 to 291 hours and cumulative rainfall ranging from 5.7 to 287 mm. However, most of the points are concentrated between durations of 10 to 100 hours and cumulative rainfall of 20 to 110 mm. In contrast, the majority of Alex landslides are associated with shorter rainfall durations, ranging from 24 to 37 hours, but with substantially higher cumulative rainfall, from 101 to 663 mm, reflecting the brief and intense character of Storm Alex.

When examining these Alex landslides in more detail, two distinct vertical clusters appear in the plot: a first group characterized by durations between 24 and 29 hours, and a second one with durations between 34 and 39 hours. This separation does not reflect a temporal variability in landslide occurrence, since all of these landslides are dated from October 3, but rather results from the spatial pattern of the Storm Alex. Shorter durations correspond to peripheral areas of the storm, where rainfall intensity and persistence were lower, whereas longer durations occurred mainly in areas affected by the core of the storm, where precipitation was more sustained and intense. Two Alex landslides are outside of this window, with durations of 61 and 73 hours and rainfall amounts of 205 and 162 mm, respectively. These two landslides occurred on October 4 after a minor secondary rainfall period still associated with Storm Alex.

Overall, the most notable result in Fig. 6 **is** that the threshold derived from the WSAL dataset is approximately 3 times higher than the WoSAL threshold**.** However**,** despite this vertical offset, both thresholds are almost parallel. As a consequence, it is observed that 172 landslides fall below the WSAL threshold, all of which correspond to non-Alex landslides. In contrast, only 28 landslides fall below the WoSAL threshold. Finally, the WSAL threshold presents significantly larger uncertainties than the WoSAL threshold.

Recall that the default hour of occurrence is set at 12:00 in the CTRL-T algorithm. To assess the influence of this arbitrary choice, sensitivity tests were performed by changing the assumed landslide occurrence time (00:00, 06:00, 12:00, 18:00, and 23:00) (Fig. A3). This resulted in noticeable changes in the obtained thresholds. However, in all cases, the threshold including the Alex landslides remained significantly higher than the threshold computed without them, by a factor of 2.8 to 3.5.

https://doi.org/10.5194/egusphere-2026-458
Preprint. Discussion started: 4 February 2026

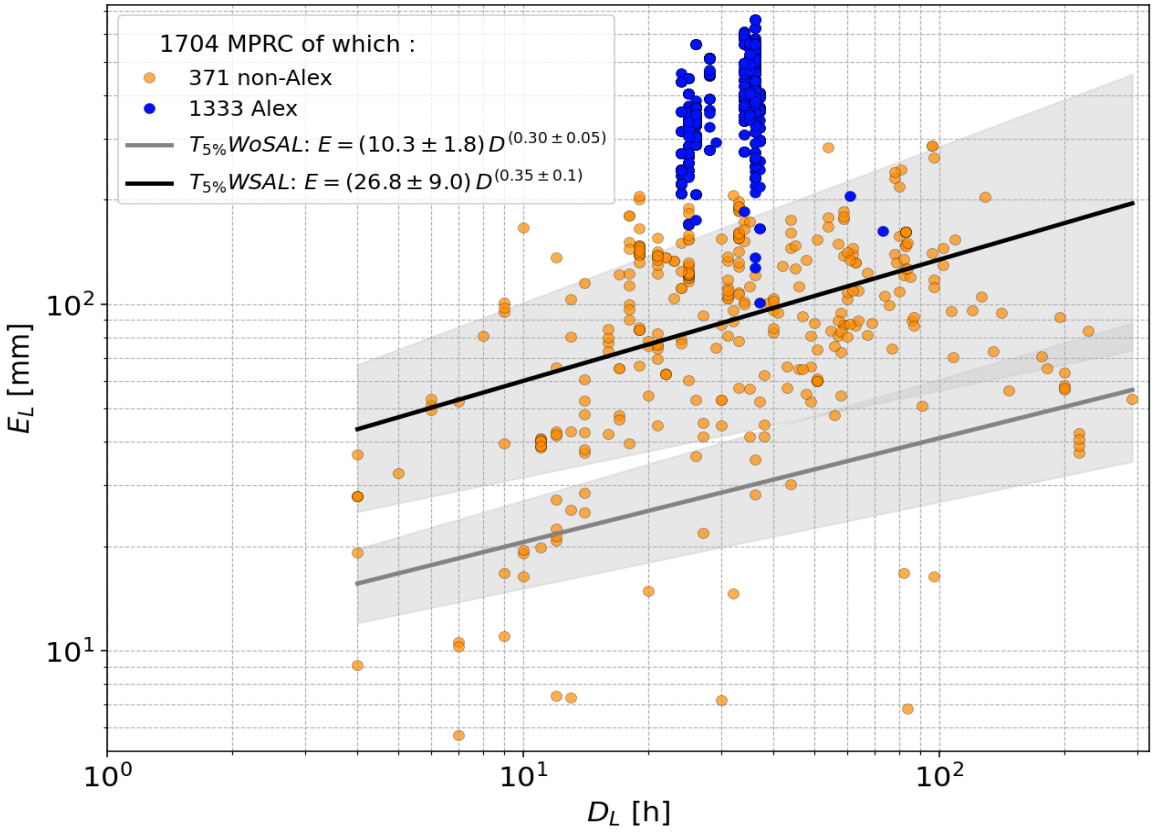

Figure 6: ED thresholds calculated under MPRC conditions (Most Probable Rainfall Conditions). The x-axis represents the duration (h) of the rainfall from the beginning of the rainfall event until the occurrence of the landslide, and the y-axis represents the corresponding amount of rainfall (mm), both in log-log scales. Blue points are associated with Alex landslides while orange points represent non-Alex landslides. The threshold computed from the WSAL and WoSAL datasets are represented in black and grey, respectively. The light grey shaded areas indicate the associated uncertainties.

5.2 Predisposing factors

5.2.1 Permutation importances

Feature importances in the RF model are presented in Fig. 7. For the WoSAL datasets (Fig. 7a), the most influential features are slope and clay content (0–30 cm), followed by landform classification according to Iwahashi and Pike, and lithology. These four factors are largely dominant, while other features such as aspect, silt content (0–30 cm), and land cover have intermediate importance. The three lowest-ranked features (landform Weiss, TPI, curvature) form a distinct group clearly separated from other features.

In contrast, for the WSAL datasets (Fig. 7b), clay content (0–30 cm) becomes the most influential feature, followed very closely by slope. Silt and sand content over 0–30 cm gain in importance compared to the WoSAL case and are placed just behind. Lithology still makes a significant contribution. The importance of landform according to Iwahashi and Pike

https://doi.org/10.5194/egusphere-2026-458
Preprint. Discussion started: 4 February 2026

markedly decreases, falling to seventh place. Similarly to the WoSAL dataset, landform (Weiss), TPI and curvature remain the least influential features, forming a distinct group with consistently low importance scores.

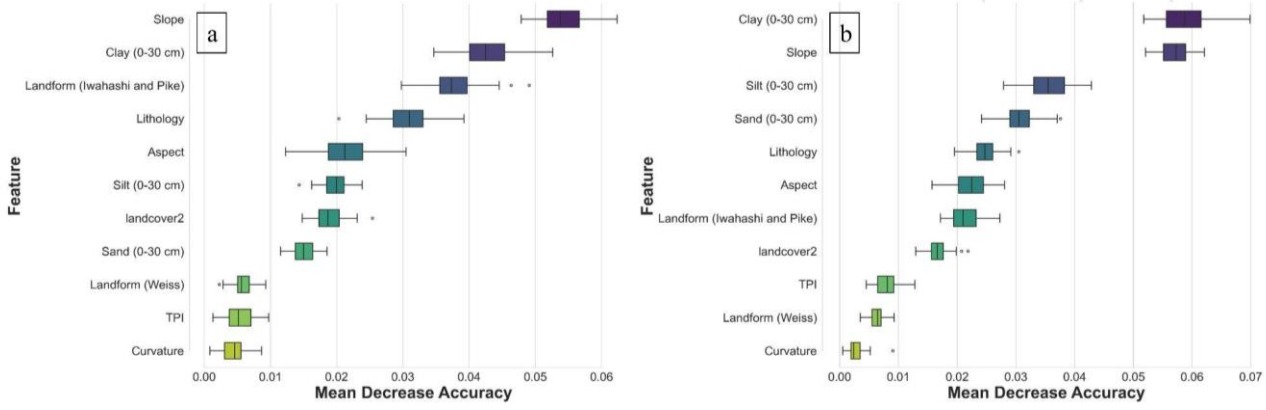

Figure 7: Permutation importances obtained for predisposing factors (a) with the WoSAL datasets (b) with the WSAL datasets.

5.2.2 Comparative analysis of slope, clay content and lithology

As shown in Fig. 7, slope, clay content and lithology are among the most influential factors for landslide initiation in our study area (Guzzetti et al., 1996; Reichenbach et al., 2018; Xu et al., 2012). The distributions of these three factors for Alex and non-Alex landslides are compared in Fig. 8.

The distributions of slope angle for Alex and non-Alex landslides show a unimodal shape, with most landslides occurring between 20° and 40° (Fig. 8a). The distribution of Alex landslides appears slightly shifted towards lower values, with an average slope of 30°. In contrast, non-Alex landslides show a slightly higher average slope of 32°. Approximately 52% of Alex landslides occurred on slopes below 30°, compared to 44% for non-Alex landslides. Both distributions show a marked decrease for slope angles higher than 45°, even more pronounced for Alex landslides.

Fig. 8b shows the distribution of clay content (%) in the upper 0–30 cm of the soil for Alex and non-Alex landslides. Both distributions are centered around 20% clay content. However, non-Alex landslides exhibit a higher peak in probability density at this value. Alex landslides more frequently affect areas with lower clay content, with approximately 10% of Alex landslides occurring in soils with clay content below 18%, compared to only about 2% for non-Alex landslides. This indicates that Alex landslides were triggered in less clay-rich terrains.

Fig. 8c presents the lithological ratios (LR) calculated for both Alex and non-Alex landslides that occurred in the post-Alex ortho-express zone (red outlines in Fig. 3). For each lithological class, this ratio corresponds to the proportion of landslides in that class, normalized by the surface proportion of the class within the post-Alex ortho-express zone. For non-Alex landslides, the *marls* lithology stands out with a much higher ratio (LR = 7.7) than other classes. Five lithologies exhibit moderate LR ratios, ranging from 2.7 to 1.2: *limestone and others*, *gypsum*, *cargneules and clay*, *fluvial deposits*, *conglomerates and others*, and *heterogeneous slope deposits*. The eleven other lithologies show low ratios (LR < 1). In

https://doi.org/10.5194/egusphere-2026-458
Preprint. Discussion started: 4 February 2026

contrast, Alex landslides exhibit a different lithological distribution. Four lithologies are predominant: *gneiss*, *flysch*, *marls*, and *fluvio-glacial deposits* (LR between 3.3 and 4.4). The lithologies *gypsum, cargneules and clay*, *marly limestone*, *anthropogenic deposits*, *heterogeneous slope deposits*, *moraines*, and *fluvial deposits* show intermediate LR ratios, ranging from 2.0 to 1.1. Finally, the eleven remaining lithologies have LR ratios below 1, including *limestone and others* which show a higher LR ratio for non-Alex landslides.

The analysis highlights clear disparities between Alex landslides, triggered by a millennial return period rainfall event, and non-Alex landslides, caused by less intense precipitation events. The results indicate that Alex landslides occurred on slightly gentler slopes than non-Alex landslides. In terms of soil texture, Alex landslides more frequently affected areas with lower clay content. Also, while some lithologies show similar low involvement in both groups, most lithological classes responded differently to Storm Alex. In particular, some lithological classes were mobilized exclusively during Storm Alex, as *fluvio-glacial deposits*, *anthropogenic deposits*, *flysch*, and *gneiss*. Conversely, *magmatic and plutonic rocks*, and *calcareous marls* exclusively appear for non-Alex landslides. Overall, this lithological analysis suggests that lithologies respond differently depending on the intensity of the triggering rainfall events.

https://doi.org/10.5194/egusphere-2026-458
Preprint. Discussion started: 4 February 2026

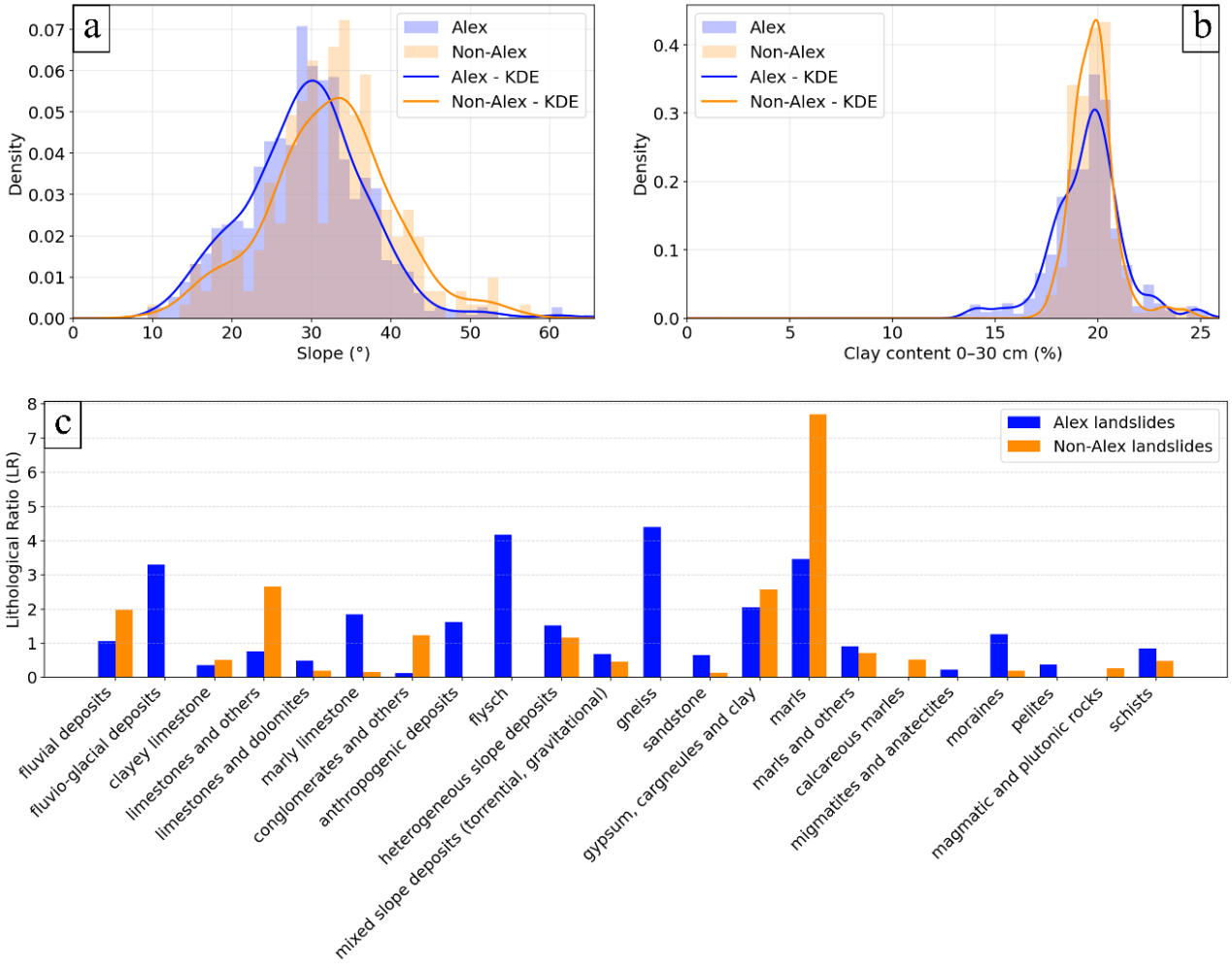

Figure 8: Distribution of (a) slope angles (°) and (b) clay content (%) represented by density-normalized histograms and kernel density estimation (KDE) curves for Alex landslides (blue) and non-Alex landslides (orange). The x-axis shows slope angle and clay content, respectively, while the y-axis represents the probability density, i.e. the relative frequency at which landslides occurred for a given slope angle or clay content. (c) Comparison of lithological ratios (LR) between Alex and non-Alex landslides within the post-Alex Ortho-Express area. LR indicates how frequently landslides occurred in each lithological class relative to the surface coverage of that class. Blue bars correspond to Alex landslides, whereas orange bars represent non-Alex landslides.

5.2.3 Landslide susceptibility maps

Fig. 9a and 9b show the mean susceptibility maps calculated from the WoSAL and WSAL datasets, respectively. The susceptibility values are discretized into six classes to facilitate comparison. Both maps exhibit strong spatial variability. Low values (≤ 0.1) are typically found in the plains, while higher values occur predominantly in areas of pronounced relief located in the northern part of the department. The highest susceptibility values (> 0.9) are found in the municipality of Menton on both maps, as shown in the zoomed areas in Fig. 9c and 9d. This observation reflects the large number of landslides recorded in the municipality of Menton (see also Fig. 11c).

https://doi.org/10.5194/egusphere-2026-458
Preprint. Discussion started: 4 February 2026

The statistical distribution of susceptibility values for both maps is presented on Fig. 10. Overall, both distributions show similar shapes. In both cases, a prominent peak appears near 0, indicating a high number of pixels with very low susceptibility values. Overall, pixels with susceptibility below 0.1 account for 13% and 16% of the total in the WoSAL and WSAL maps, respectively. A secondary peak in the distribution appears around 0.4, slightly more pronounced in the WoSAL distribution. Overall, 33% and 30% of pixels fall within the 0.3–0.5 range for the WoSAL and WSAL maps, respectively. Above 0.4, both distributions show a marked decline. Susceptibility values above 0.8 are extremely rare: less than 0.3% of pixels exceed this value in both maps.

To better illustrate the impact of Alex landslides, a difference map is generated by subtracting the WoSAL map from the WSAL map (Fig. 11). Overall, the differences range from −0.2 to 0.6. About 72% of the territory presents a negative difference, while 28% show an increase in susceptibility. Large difference values are rare, as 94% of the territory shows a difference between −0.1 and 0.1, and about 16% presents no significant difference (between −0.01 and 0.01). Susceptibility increases are mainly located near the locations of the Alex landslides, as shown in the Vesubie Valley in Fig 11a. However, susceptibility increases are also observed in areas where no Alex landslides were recorded, as visible in the eastern part of the Roya valley in Fig. 11b. The municipality of Menton exhibits a small decrease in susceptibility (Fig. 11c) but the values remain nevertheless very high in the area (see zoom in Fig. 9c and 9d). This decrease reflects the fact that, proportionally, the majority of Alex landslides occurred in other locations.

https://doi.org/10.5194/egusphere-2026-458
Preprint. Discussion started: 4 February 2026

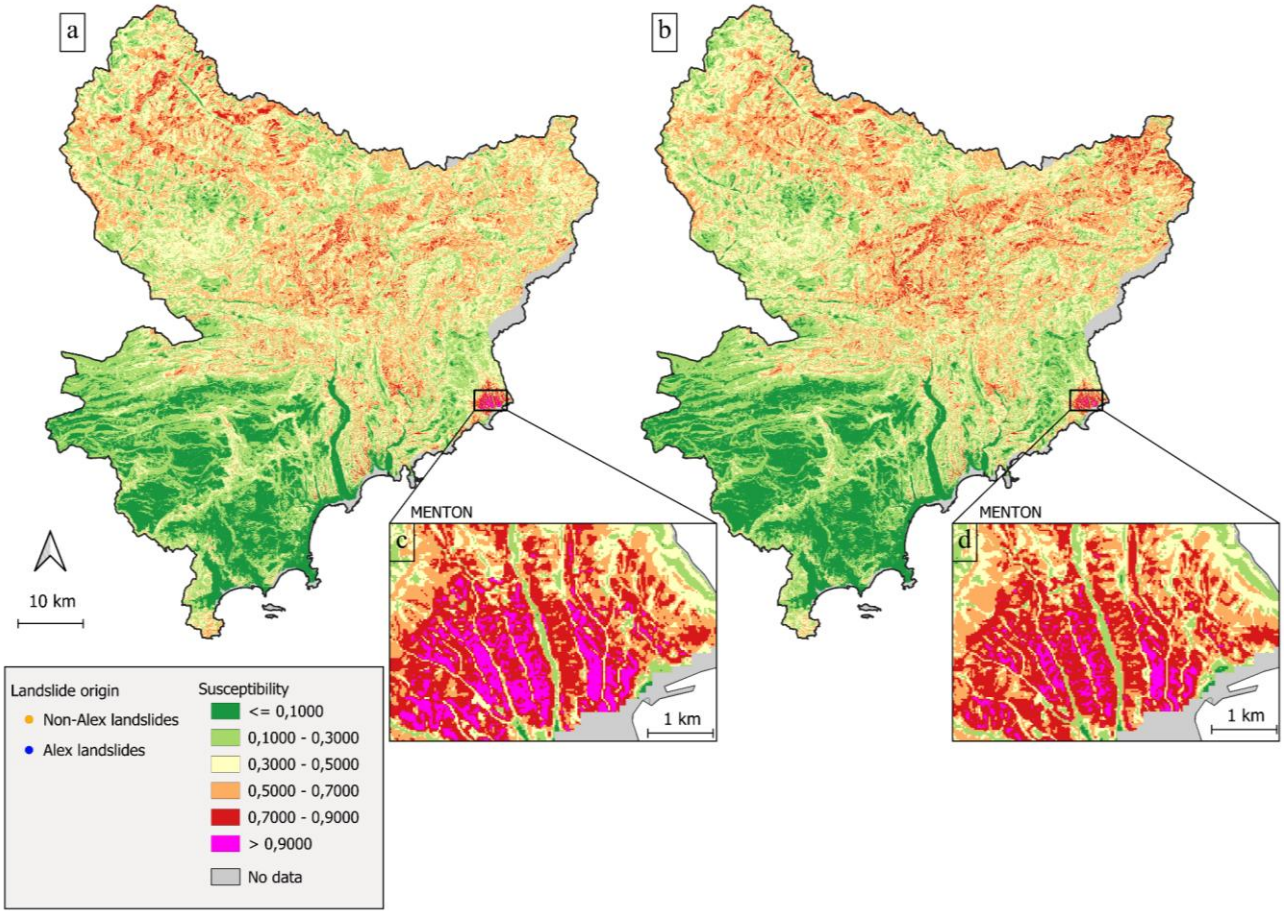

Figure 9: Susceptibility maps computed from (a) the WoSAL dataset, and (b) the WSAL dataset. Insets (c) and (d) show close-ups on the municipality of Menton.

https://doi.org/10.5194/egusphere-2026-458
Preprint. Discussion started: 4 February 2026

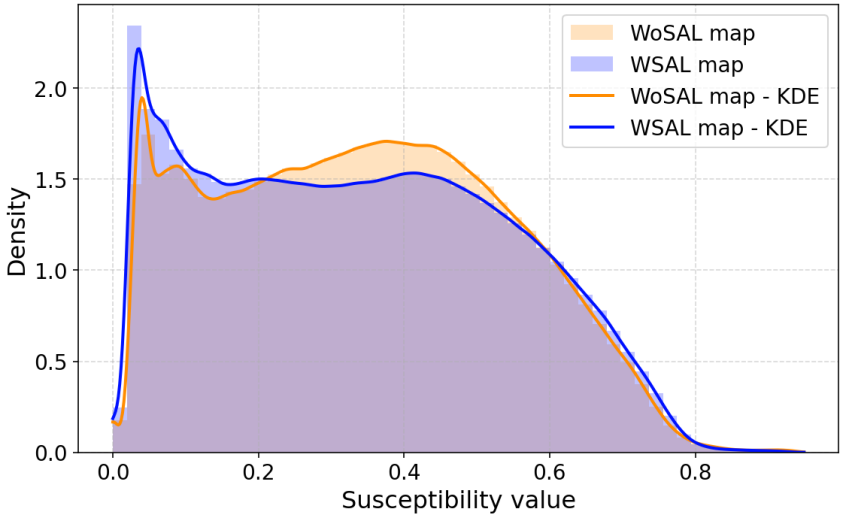

Figure 10: Kernel density estimation (KDE) of the distributions of susceptibility values for all pixels in the WSAL (blue) and WoSAL (orange) maps.

https://doi.org/10.5194/egusphere-2026-458
Preprint. Discussion started: 4 February 2026

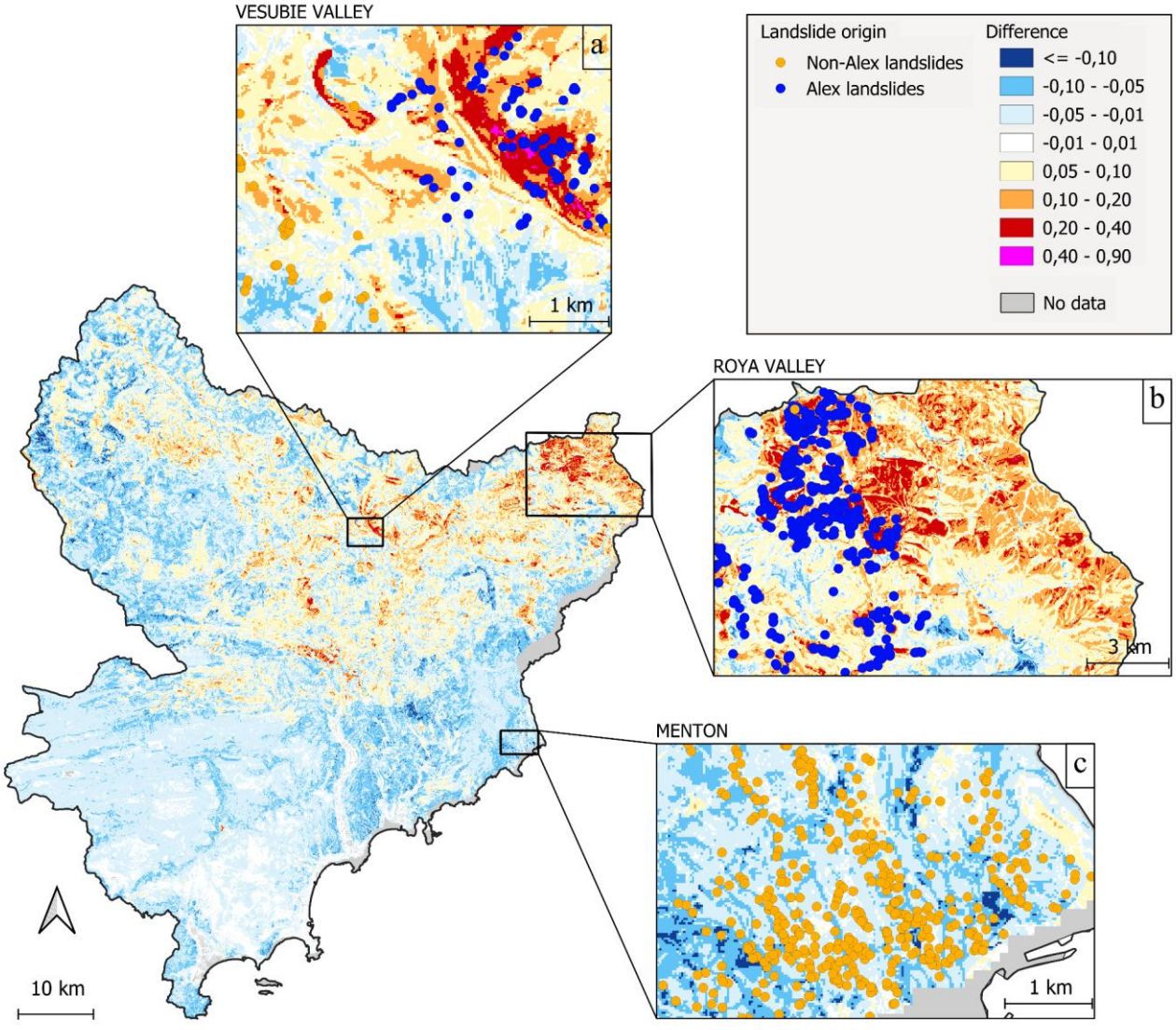

Figure 11: Difference of the two susceptibility maps (WSAL - WoSAL). Positive values (red areas) correspond to an increase in susceptibility after integrating Alex landslides, while negative values (blue areas) indicate a decrease in susceptibility. Blue points correspond to location Alex landslides while orange points represent non-Alex landslides. Three insets show close-up views of (a) the Vésubie Valley, (b) the northern part of the Roya Valley, and (c) the municipality of Menton.

5.2.4 Susceptibility values for Alex and non-Alex landslides

Figure 12 shows the distributions of susceptibility values at the locations of Alex and non-Alex landslides. For both distributions, susceptibility values were extracted from the WoSAL map (computed without Alex landslides). The two curves display pronounced differences. Non-Alex landslides present a distribution centered on high values, with a mean susceptibility of 0.76, and values ranging from 0.37 to 0.95. Conversely, Alex landslides show a wider distribution with a

https://doi.org/10.5194/egusphere-2026-458
Preprint. Discussion started: 4 February 2026

plateau between 0.5 and 0.7, a mean of 0.54, and values spanning from 0.05 to 0.81. Overall, Alex landslides tended to occur in areas with lower susceptibility values than non-Alex landslides. This result suggests that the predisposing configurations learned by the RF model from landslides associated with non-extreme rainfall does not entirely capture the predisposing patterns associated with extreme events. It is also observed that no Alex landslide occurred for susceptibility values above 0.8. This surprising result actually reflects the fact that there are no areas with susceptibility greater than 0.8 in the area affected by Storm Alex (not shown).

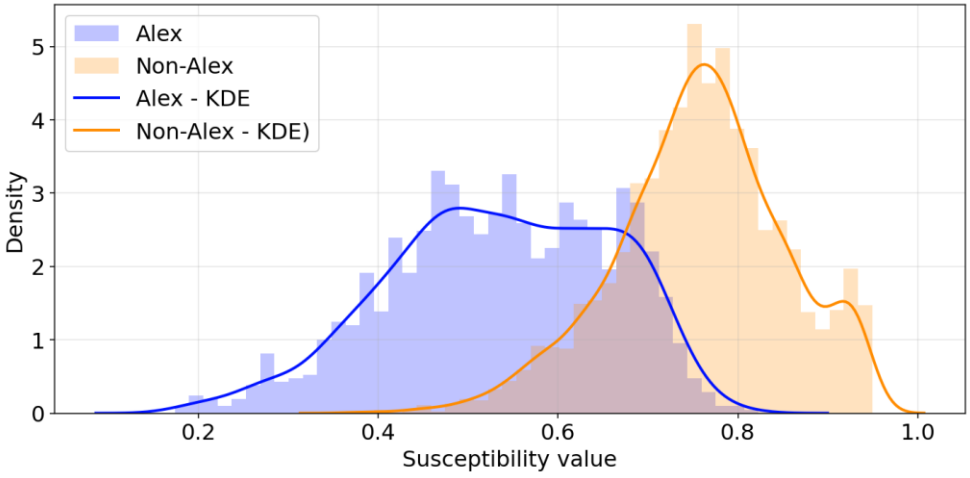

Figure 12: Kernel density estimates (KDE) distributions of susceptibility values at the locations of Alex (blue) and non-Alex (orange) landslides on the WoSAL map. Dashed lines indicate the means of each distribution.

6 Discussion

Using an inventory of 5,383 shallow landslides in the Alpes-Maritimes region, including 1,655 events triggered by the millennial Storm Alex (October 2020), this study shows that the inclusion of landslides triggered by extreme rainfall events substantially alters both rainfall–duration thresholds and susceptibility patterns. ED thresholds computed with Storm Alex landslides are increased by a factor of approximately 2.8 to 3.5 compared to thresholds derived from more common events. Susceptibility maps based on RF modelling reveals that Storm Alex landslides occurred under different predisposing conditions, and in areas characterized by a lower pre-event susceptibility. Incorporating Alex landslides modifies the spatial distribution of susceptibility, locally increasing values in areas sharing similar predisposing conditions, while slightly decreasing susceptibility elsewhere.

6.1 Quality of landslide inventory

Approximately 97% of Alex landslides were identified by orthophotography comparison and field analysis, ensuring a very good (decametric) spatial accuracy. In contrast, only 68% of non-Alex landslides were mapped using the same approach. To reduce this disparity, landslide locations were checked and adjusted whenever possible using textual information. Due to

https://doi.org/10.5194/egusphere-2026-458
Preprint. Discussion started: 4 February 2026

incomplete information, it is possible that a very small number of landslides with a spatial accuracy indicated as decametric have in fact an erroneous location. However, this concerns a minority of landslides and does not affect the results of ED thresholds and susceptibility analyses.

The temporal accuracy of the landslide inventory is also important for the ED threshold analysis. Approximately 43% of the landslides inventory have an hourly or daily temporal accuracy (Fig. 3d), ensuring that the thresholds can be computed based on a sufficient number of events. Note that all these landslides are dated on 3 October, although some of them may have occurred on 2 October during the storm itself. Consequently, the WSAL threshold should be considered as an upper bound, assuming that the whole storm Alex cumulative rainfall has contributed to the landslides. However, the sensitivity tests performed on landslide time occurrence ascertain that the difference between the WSAL and WoSAL thresholds is a robust result.

6.2 Impact of Storm Alex landslides on rainfall triggering thresholds

Although numerous recent studies have addressed empirical ED thresholds for shallow landslides, the influence of including storm-induced landslides and the implications for operational threshold design have received little attention. The difference between the WSAL and WoSAL thresholds is explained by the exceptional character of Storm Alex, which produced extreme rainfall accumulation and a large number of landslides over a short time window, therefore shifting the statistical relationship between rainfall and landslide occurrences towards higher values. Including such extreme events in the calculation of thresholds therefore reduces their sensitivity to more “common” rainfall events. This could lead to a higher rate of missed alarms, as illustrated by the larger number of landslides falling below the threshold (172) when Alex landslides are included compared to 28 when they are excluded (Fig. 6). However, it should be noted that in Fig. 6, all the points corresponding to Storm Alex significantly exceed the thresholds calculated without their inclusion. In practice, this means that a threshold calibrated with non-extreme events is effective at predicting the occurrence of landslides in a context of extreme rainfall.

However, for operational use, it should also be kept in mind that these thresholds could also lead to a high rate of false alarms. Several studies have demonstrated that when rainfall intensity exceeds soil hydraulic conductivity, runoff moderates the effect of rainfall on slope stability, such that the critical stability threshold is reached less quickly (Suradi et al., 2016; Ran et al., 2018; Zhang et al., 2022). In other words, the instability of slopes is not always directly correlated to rainfall intensity in particular for exceptional rainfall events such as storm Alex. This could argue for including additional parameters in the definition of thresholds for extreme events such as e.g. the rainfall intensity, the return period, or the effective rainfall (the rainfall infiltrated in the soil).

This study is based on a 5% non-exceedance probability for the computation of ED thresholds. It has been demonstrated that the selected non-exceedance probability strongly influences the balance between missed and false alarms, i.e., between the sensitivity and reliability of the thresholds (Barthélemy et al., 2024). In the present case, considering Alex landslides implies a decrease in the conservativeness of the threshold, as 14% of non-Alex landslides fall below the WSAL threshold. Choosing

https://doi.org/10.5194/egusphere-2026-458
Preprint. Discussion started: 4 February 2026

more conservative probability levels could help enhancing the reliability of the WSAL threshold. In fact, when considering Alex landslides, a non-exceedence probability of about 0.5% is required to obtain a threshold comparable to the 5% WoSAL threshold. In general, it could be suggested to adapt the non-exceedance probability to the return period of the rainfall events considered in the analysis. It should also be mentioned that considering extreme events may invalidate the assumption of normal distribution of the residuals in the CTRL-T algorithm, and thus the determination of the thresholds.

Finally, in our analysis, one data point is assigned to each landslide regardless of whether several landslides are associated with the same rainfall event. This approach can lead to a strong imbalance between Alex and non-Alex-induced landslides. This imbalance, combined with the extreme rainfall associated with Storm Alex contributes to the significantly higher level of the WSAL threshold. Approaches based on event clustering could help reduce this excessive weighting of Alex landslides (Benz and Blum, 2019).

6.3 Interpretation of susceptibility scores

Random Forest (RF) is a supervised machine learning algorithm. Although RF is generally considered robust (Goetz et al., 2015), the performance of the algorithm is sensitive not only to the quality and structure of the input data but also to the choice of hyperparameters (Catani et al., 2013). This sensitivity arises because RF is a data-driven algorithm whose decisions reflect the empirical distribution of conditioning factors in the observations, rather than mechanical processes of slope failure. These characteristics are particularly important in the context of susceptibility mapping, since RF outputs reflect the empirical distribution of conditioning factors in the observations, rather than mechanical processes of slope failure. In our case, the considered susceptibility scores correspond to the proportion of trees predicting a landslide occurrence for a given pixel. These scores should not be interpreted as absolute probabilities of failure, but rather as a relative index of similarity between the environmental conditions of the pixels on the map and those assigned to landslides. In general, however, identifying areas sharing similar conditions with past landslides is the fundamental principle of susceptibility mapping. The fact that the model presents high predictive performances demonstrates that this similarity index is operationally relevant, as it is able to identify unstable configurations that are not present in the calibration set, and can effectively be interpreted as susceptibility score.

6.4 Changes in susceptibility maps due to Storm Alex landslides

The use of RF allowed us to compute two susceptibility maps, with and without including Alex landslides. The high performance scores in Table 2 demonstrate that the RF has a strong generalization capability, i.e. that it can accurately predict landslides that were not included in its training datasets. This is also illustrated by the spatial distribution of the susceptibility, where high values (>0.5) occur not only in areas where landslides have been recorded, but also in potentially susceptible zones without any known landslides, as shown in the Roya Valley (Fig. 9). The fact that a majority of the Alex landslides are well captured in the WoSAL susceptibility map (60.5% of Alex landslides having a susceptibility higher than 0.5) also demonstrate the robustness and reliability of the model.

https://doi.org/10.5194/egusphere-2026-458
Preprint. Discussion started: 4 February 2026

Overall, the changes between the two maps remain moderate (94% of the observed differences fall between -0.1 and 0.1). However, comparing the two maps reveals clear differences in susceptibility patterns. The zones where susceptibility increases after integrating Alex landslides are primarily located where these landslides occurred, or in areas with similar predisposing conditions that were not directly affected by the storm. By including numerous Alex landslides, the RF model learned new combinations of variables associated with landslide initiation under extreme rainfall events. As a consequence, however, susceptibility also slightly decreased in 72% of the territory, because the inclusion of Alex landslides weakened the statistical signal of the pre-existing predisposing patterns. Therefore, the observed differences between the two maps are not only consequences of adding new landslides, but also reflect how the model internally redefines what constitutes a susceptible environment, once exposed to landslides generated under extreme, atypical conditions. Such changes demonstrate that the inclusion of Alex landslides has a tangible impact on the resulting susceptibility patterns, with potential consequences for operational management.

These spatial variations of susceptibility are supported by the analysis of distributions of slope angles, lithologies and clay content, which show significant differences between Alex and non-Alex landslides. During Storm Alex, landslides tended to occur on slightly gentler slopes and more frequently affected areas with lower clay content (<18%), and some lithological units being more affected than others. This indicates that landslides triggered by Storm Alex developed under different geomorphological and lithological conditions. This observation explains that on average Alex landslides occurred in areas with lower susceptibility values (0.54) compared to non-Alex landslides (0.76), with the WoSAL susceptibility map as reference. The exceptional rainfall intensity associated with Storm Alex lowered the predisposition threshold required to trigger landslides, causing events in areas considered as less susceptible.

The analysis of feature importance highlights that soil texture parameters such as clay, sand and silt content are among the most influential predictors, particularly when including Alex landslides. The increased importance of these features after integrating the Alex landslides suggests that soil texture plays a more prominent role under extreme conditions, due to their influence on water infiltration and retention as well as on the mechanical properties of soil. This further supports the idea that exceptional triggering conditions can amplify the influence of certain predisposing factors.

Overall, these results are consistent with the fact that landslide initiation results from a combination of predisposing factors (such as geology, topography, land use, etc.) and triggering variables, mainly related to rainfall (Corominas et al., 2014; Ran et al., 2018; Lombardo et al., 2020; Moreno et al., 2024; Steger et al., 2024). They show the limitations of approaches for which landslides are predicted based on predisposing factors only, particularly for extreme rainfall events. A promising prospect to produce more reliable and accurate predictive models, could be to jointly consider predisposing and triggering conditions, thereby enabling the model to recognize potentially unstable configurations even under unusual conditions.

https://doi.org/10.5194/egusphere-2026-458
Preprint. Discussion started: 4 February 2026

7 Conclusions

This study examines how extreme rainfall events affect the development of rainfall–duration (ED) thresholds and susceptibility maps for shallow landslides. The analysis relies on an inventory of 5,383 shallow landslides, of which 1,655 were directly triggered by Storm Alex (October 2, 2020), a rainfall event with an estimated millennial return period. The objective is to determine to what extent the inclusion of landslides triggered by this storm modifies the statistical models commonly used for hazard assessment and mapping. The CTRL-T algorithm was applied to calculate and compare ED thresholds constructed with and without Storm Alex-induced landslides. A Random Forest (RF) method was used to generate and compare susceptibility maps constructed with or without these landslides. Particular attention was paid to the impact of non-landslide points on the outputs.

The results reveal several key findings. First, the inclusion of landslides associated with Storm Alex leads to a substantial increase in the ED threshold, by up to a factor of 3.5, compared to that established using only the other landslides in the inventory. This increase reflects the extreme nature of the storm and highlights the high sensitivity of statistical approaches to the presence of rare events. Incorporating such events into the statistical threshold calculations therefore reduces their sensitivity to more common rainfall events and could increase the rate of missed alerts. Conversely, thresholds calibrated without the storm-induced landslides maintain a very good predictive capacity for extreme rainfall, emphasizing the importance of distinguishing between ordinary and exceptional rainfall regimes when defining operational thresholds.

Second, the comparative analysis of the distributions of predisposing factors (slope, clay and lithology) between Alex and non-Alex landslides, together with the susceptibility maps produced using the RF method, indicates that landslides triggered by Storm Alex occurred under predisposing conditions that differ from those associated with more recurrent events. On average, the storm-induced landslides developed on slightly gentler slopes, more frequently impacted terrains with lower clay contents (<18%), affected specific lithologies, and occurred in areas with lower susceptibility values. Such differences suggest that the exceptional rainfall intensity associated with Storm Alex lowered the stability threshold of slopes. Accordingly, the inclusion of these events in the RF training dataset altered the statistical relationships between predisposing factors and landslide occurrence, resulting in a susceptibility increase in localized areas but in an overall susceptibility decrease elsewhere. This demonstrates that extreme events do not simply add more data points to the inventory, but that they reshape susceptibility patterns, and have serious implications for the robustness of statistical models and operational risk management.

These findings have implications that extend beyond our local case study, contributing to the broader understanding of the limits and applicability of data-driven landslide prediction models when extreme cases are considered. More specifically, this work highlights that (i) inventories containing landslides triggered during rare rainfall event should be considered carefully, (ii) landslide predictive tools based on statistical and machine-learning behave differently under exceptional forcing conditions and (iii) methodologies developed using more common events cannot always be directly extrapolated to

https://doi.org/10.5194/egusphere-2026-458
Preprint. Discussion started: 4 February 2026

rare events. In the context of climate change, where the frequency and intensity of extreme rainfall events are expected to increase, we believe that these conclusions can help to design more effective predictive tools.

From a methodological perspective, several prospects emerge from this study. First, the analysis points out the importance of jointly considering predisposing (e.g., slope, lithology, land use) and triggering factors (e.g., rainfall intensity and duration) in landslide susceptibility assessment. Statistical models integrating both predisposing factors and triggering variables would presumably better capture the full range of conditions under which landslides occur, thereby improving hazard assessment and risk management strategies. Secondly, incorporating additional parameters, such as antecedent soil moisture, snowmelt indicators, or effective rainfall rather than event-based rainfall metrics, could further enhance the predictive capability of these models. Finally, performing analyses by landslide type (e.g., riverbank landslides, flow-like landslides, mid-slope landslides and cut-slope landslides) is also relevant, as different processes are controlled by distinct conditioning and triggering mechanisms; however, such stratification inevitably reduces the number of available landslides for model calibration and validation, potentially limiting statistical robustness and requiring larger or longer-term inventories.

2 Appendices

https://doi.org/10.5194/egusphere-2026-458
Preprint. Discussion started: 4 February 2026

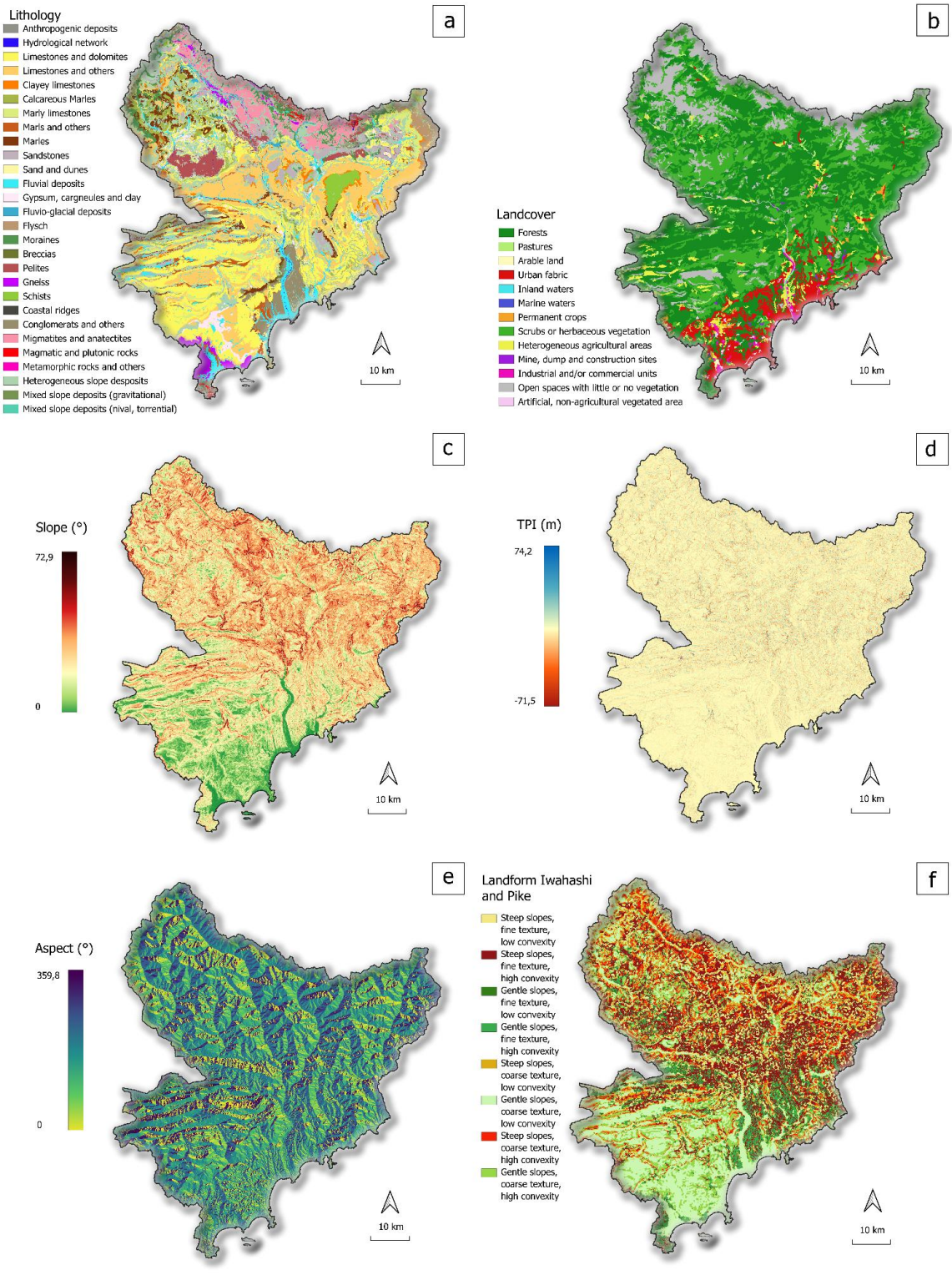

https://doi.org/10.5194/egusphere-2026-458
Preprint. Discussion started: 4 February 2026

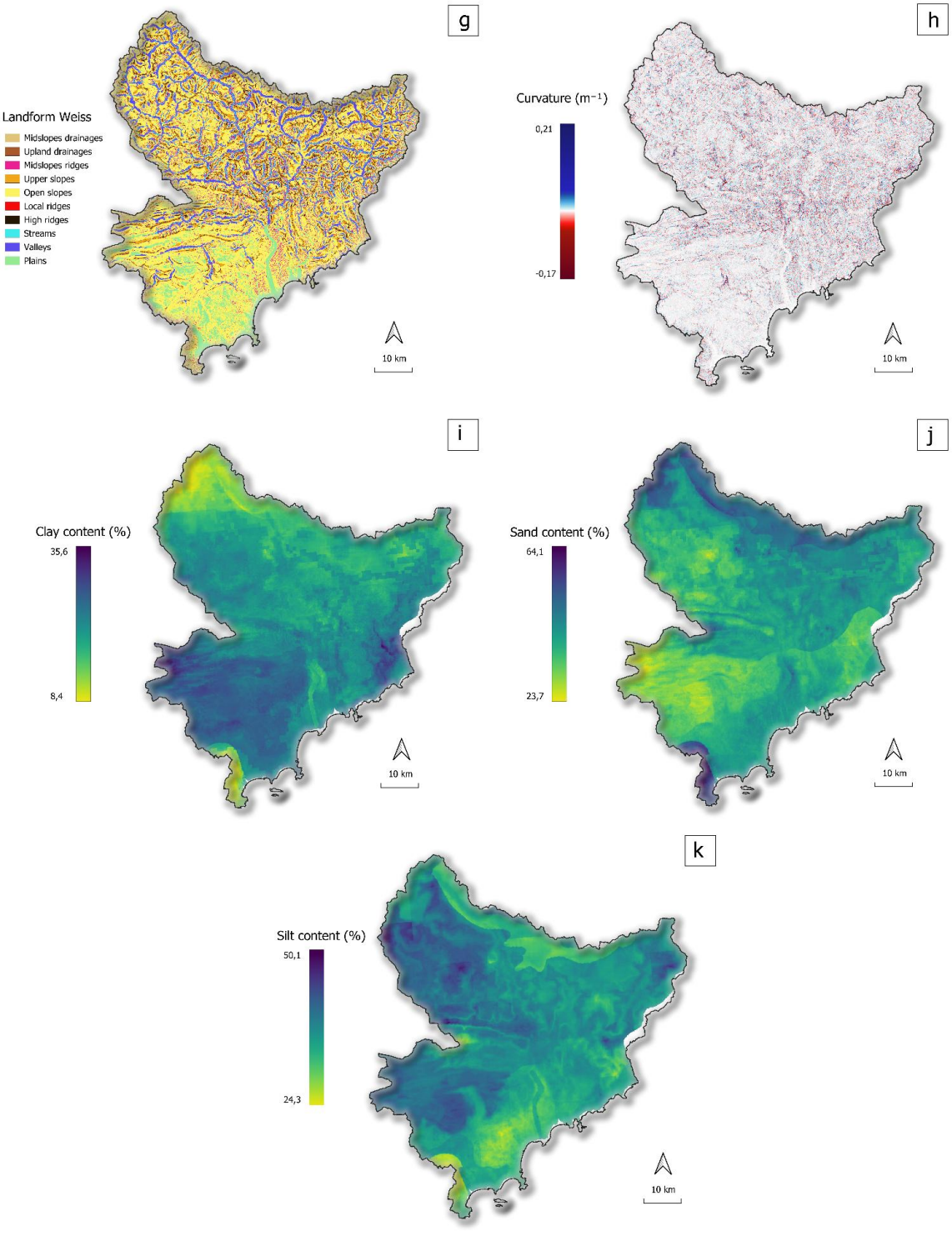

https://doi.org/10.5194/egusphere-2026-458
Preprint. Discussion started: 4 February 2026

Appendix A1: Landslide predisposing factors : a Lithology; b Corine Landcover; c Landform of Iwashi and Pike; d Landform of Weiss; e Slope angle; f Topographic Position Index (TPI); g Aspect; h Curvature; i Clay content over 0-30 cm depth; j Sand content over 0-30 cm depth; k Silt content over 0-30 cm depth.

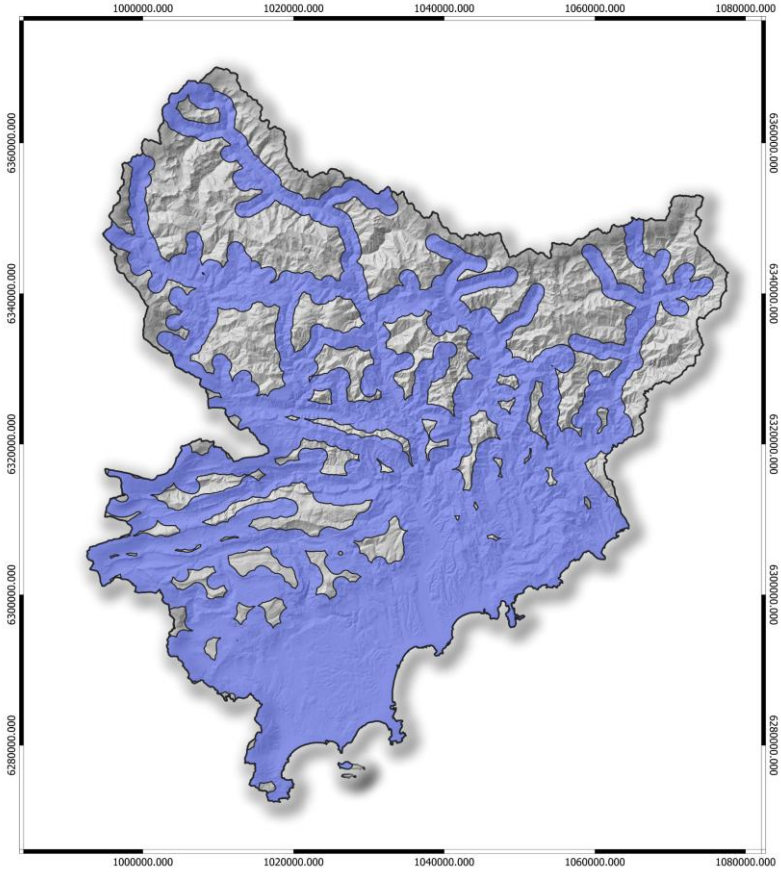

Appendix A2: Definition of the valid area (shown in light blue) used for generating non-landslide samples, corresponding to a 1 km buffer around major roads, excluding zones within 150 m of recorded landslides.

https://doi.org/10.5194/egusphere-2026-458
Preprint. Discussion started: 4 February 2026

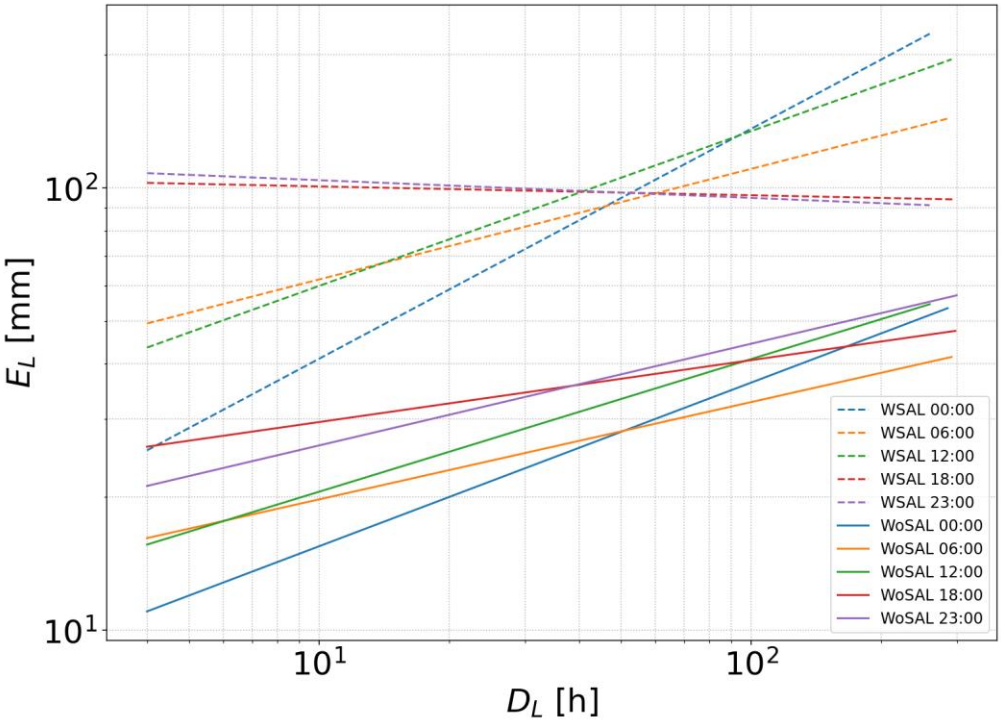

Appendix A3: ED thresholds calculated according to different hours of occurrence for landslides. Solid lines correspond to WoSAL thresholds, while dashed lines indicate WSAL thresholds. Line colours represent the triggering hour of landslides (00:00, 06:00, 12:00, 18:00, and 23:00).

Data availability

COMEPHORE meteorological data are available on the following portal: https://www.data.gouv.fr/.

Landslide data will be made available upon request.

Author contributions

Conceptualization, Methodology, Writing : LA, GC, SB, OC, YT, NS

Resources: YT, NS, NM, LF

Supervision: GC, SB, OC

Competing interests

The authors have no competing interests to declare that are relevant to the content of this article.

https://doi.org/10.5194/egusphere-2026-458
Preprint. Discussion started: 4 February 2026

Disclaimer

Copernicus Publications adds a standard disclaimer: "Copernicus Publications remains neutral with regard to jurisdictional claims made in the text, published maps, institutional affiliations, or any other geographical representation in this paper. While Copernicus Publications makes every effort to include appropriate place names, the final responsibility lies with the authors. Views expressed in the text are those of the authors and do not necessarily reflect the views of the publisher."
Please feel free to add disclaimer text at your choice, if applicable.

Acknowledgements

We thank Jérémy Rohmer (BRGM) for his valuable advice on statistical methods, particularly regarding the Random Forest algorithm.

Financial support

This work is funded by the ANR VIGIMONT project (ANR-22-CE04-0021) and by France 2030 IRIMONT project (ANR-22-EXIR-0003).

Review statement

The review statement will be added by Copernicus Publications listing the handling editor as well as all contributing referees according to their status anonymous or identified.

References

Achu, A.L., Thomas, J., Aju, C.D., Vijith, H., Gopinath, G., 2024. Redefining landslide susceptibility under extreme rainfall events using deep learning. Geomorphology 448, 109033. https://doi.org/10.1016/j.geomorph.2023.109033

Altmann, A., Toloşi, L., Sander, O., Lengauer, T., 2010. Permutation importance: a corrected feature importance measure. Bioinformatics 26, 1340–1347. https://doi.org/10.1093/bioinformatics/btq134

Arbizzi, S., Scinotti, B., Desbouis, J.-F., Moreau, L., Sauzey, P., Vilmus, F., 2021. Retour d'expérience des intempéries des 2 et 3 octobre 2020 dans les Alpes Alpes-Maritimes.

Armaş, I., Vartolomei, F., Stroia, F., Braşoveanu, L., 2014. Landslide susceptibility deterministic approach using geographic information systems: application to Breaza town, Romania. Nat. Hazards 70, 995–1017. https://doi.org/10.1007/s11069-013-0857-x

Barthélemy, S., Bernardie, S., Grandjean, G., 2024. Assessing rainfall threshold for shallow landslides triggering: a case study in the Alpes Maritimes region, France. Nat. Hazards. https://doi.org/10.1007/s11069-024-06941-2

https://doi.org/10.5194/egusphere-2026-458
Preprint. Discussion started: 4 February 2026

Bebi, P., Bast, A., Ginzler, C., Rickli, C., Schöngrundner, K., Graf, F., 2019. Forest dynamics and shallow landslides: a large-scale GIS-analysis. Schweiz. Z. Forstwes. 170, 318–325. https://doi.org/10.3188/szf.2019.0318

Benz, S.A., Blum, P., 2019. Global detection of rainfall-triggered landslide clusters. Nat. Hazards Earth Syst. Sci. 19, 1433–1444. https://doi.org/10.5194/nhess-19-1433-2019

Breiman, L., 2001. Random Forest. Mach. Learn. 45, 5–32. https://doi.org/10.1023/A:1010933404324

Brunetti, M.T., Peruccacci, S., Rossi, M., Luciani, S., Valigi, D., Guzzetti, F., 2010. Rainfall thresholds for the possible occurrence of landslides in Italy. Nat. Hazards Earth Syst. Sci. 10, 447–458. https://doi.org/10.5194/nhess-10-447-2010

Caine, N., 1980. The Rainfall Intensity - Duration Control of Shallow Landslides and Debris Flows. Geogr. Ann. Ser. Phys. Geogr. 62, 23–27. https://doi.org/10.1080/04353676.1980.11879996

Carrega, P., Michelot, N., 2021. Une catastrophe hors norme d'origine météorologique le 2 octobre 2020 dans les montagnes des Alpes-Maritimes. Physio-Géo 1–70. https://doi.org/10.4000/physio-geo.12370

Catani, F., Lagomarsino, D., Segoni, S., Tofani, V., 2013. Landslide susceptibility estimation by random forests technique: sensitivity and scaling issues. Nat. Hazards Earth Syst. Sci. 13, 2815–2831. https://doi.org/10.5194/nhess-13-2815-2013

Chen, W., Xie, X., Wang, J., Pradhan, B., Hong, H., Bui, D.T., Duan, Z., Ma, J., 2017. A comparative study of logistic model tree, random forest, and classification and regression tree models for spatial prediction of landslide susceptibility. CATENA 151, 147–160. https://doi.org/10.1016/j.catena.2016.11.032

Chochon, R., Martin, N., Lebourg, T., Vidal, M., 2022. Analysis of Extreme Precipitation During the Mediterranean Event Associated with the Alex Storm in The Alpes-Maritimes: Atmospheric Mechanisms and Resulting Rainfall, in: Gourbesville, P., Caignaert, G. (Eds.), Advances in Hydroinformatics, Springer Water. Springer Nature Singapore, Singapore, pp. 397–418. https://doi.org/10.1007/978-981-19-1600-7_26

Clapuyt, F., Vanacker, V., Christl, M., Van Oost, K., Schlunegger, F., 2019. Spatio-temporal dynamics of sediment transfer systems in landslide-prone Alpine catchments. Solid Earth 10, 1489–1503. https://doi.org/10.5194/se-10-1489-2019

Corominas, J., van Westen, C., Frattini, P., Cascini, L., Malet, J.-P., Fotopoulou, S., Catani, F., Van Den Eeckhaut, M., Mavrouli, O., Agliardi, F., Pitilakis, K., Winter, M.G., Pastor, M., Ferlisi, S., Tofani, V., Hervás, J., Smith, J.T., 2014. Recommendations for the quantitative analysis of landslide risk. Bull. Eng. Geol. Environ. 73, 209–263. https://doi.org/10.1007/s10064-013-0538-8

Cruden, D.M., Varnes, D.J., 1996. Landslide Types and Processe. Spec. Rep. - Natl. Res. Counc. Transp. Res. Board 247, 36–57.

Fell, R., Corominas, J., Bonnard, C., Cascini, L., Leroi, E., Savage, W.Z., 2008. Guidelines for landslide susceptibility, hazard and risk zoning for land use planning. Eng. Geol., Landslide Susceptibility, Hazard and Risk Zoning for Land Use Planning 102, 85–98. https://doi.org/10.1016/j.enggeo.2008.03.022

Fu, Y., Fan, Z., Li, X., Wang, P., Sun, X., Ren, Y., Cao, W., 2025. The Influence of Non-Landslide Sample Selection Methods on Landslide Susceptibility Prediction. Land 14, 722. https://doi.org/10.3390/land14040722

https://doi.org/10.5194/egusphere-2026-458
Preprint. Discussion started: 4 February 2026

Goetz, J.N., Brenning, A., Petschko, H., Leopold, P., 2015. Evaluating machine learning and statistical prediction techniques for landslide susceptibility modeling. Comput. Geosci. 81, 1–11. https://doi.org/10.1016/j.cageo.2015.04.007

Gökceoglu, C., Aksoy, H., 1996. Landslide susceptibility mapping of the slopes in the residual soils of the Mengen region (Turkey) by deterministic stability analyses and image processing techniques. Eng. Geol. 44, 147–161. https://doi.org/10.1016/S0013-7952(97)81260-4

Gonzales, G., 2008. Harmonized geological map of the Alpes-Maritimes.

Gonzalez, F.C.G., Cavacanti, M.D.C.R., Nahas Ribeiro, W., Mendonça, M.B.D., Haddad, A.N., 2024. A systematic review on rainfall thresholds for landslides occurrence. Heliyon 10, e23247. https://doi.org/10.1016/j.heliyon.2023.e23247

Gu, T., Duan, P., Wang, M., Li, J., Zhang, Y., 2024. Effects of non-landslide sampling strategies on machine learning models in landslide susceptibility mapping. Sci. Rep. 14, 7201. https://doi.org/10.1038/s41598-024-57964-5

Gu, T., Li, J., Wang, M., Duan, P., Zhang, Y., Cheng, L., 2023. Study on landslide susceptibility mapping with different factor screening methods and random forest models. PLOS ONE 18, e0292897. https://doi.org/10.1371/journal.pone.0292897

Guzzetti, F., Cardinali, M., Reichenbach, P., 1996. The Influence of Structural Setting and Lithology on Landslide Type and Pattern. Environ. Eng. Geosci. II, 531–555. https://doi.org/10.2113/gseegeosci.II.4.531

Habets, F., Boone, A., Champeaux, J.L., Etchevers, P., Franchistéguy, L., Leblois, E., Ledoux, E., Le Moigne, P., Martin, E., Morel, S., Noilhan, J., Quintana Seguí, P., Rousset-Regimbeau, F., Viennot, P., 2008. The SAFRAN-ISBA-MODCOU hydrometeorological model applied over France. J. Geophys. Res. Atmospheres 113, 2007JD008548. https://doi.org/10.1029/2007JD008548

Iverson, R.M., 2000. Landslide triggering by rain infiltration. Water Resour. Res. 36, 1897–1910. https://doi.org/10.1029/2000WR900090

Iwahashi, J., Pike, R.J., 2007. Automated classifications of topography from DEMs by an unsupervised nested-means algorithm and a three-part geometric signature. Geomorphology 86, 409–440. https://doi.org/10.1016/j.geomorph.2006.09.012

Joly, D., Brossard, T., Cardot, H., Cavailhes, J., Hilal, M., Wavresky, P., 2010. Les types de climats en France, une construction spatiale. Cybergeo. https://doi.org/10.4000/cybergeo.23155

Jones, J.N., Boulton, S.J., Bennett, G.L., Stokes, M., Whitworth, M.R.Z., 2021. Temporal Variations in Landslide Distributions Following Extreme Events: Implications for Landslide Susceptibility Modeling. J. Geophys. Res. Earth Surf. 126, e2021JF006067. https://doi.org/10.1029/2021JF006067

Lee, C.-T., Huang, C.-C., Lee, J.-F., Pan, K.-L., Lin, M.-L., Dong, J.-J., 2008. Statistical approach to storm event-induced landslides susceptibility. Nat. Hazards Earth Syst. Sci. 8, 941–960. https://doi.org/10.5194/nhess-8-941-2008

Li, B., Liu, K., Wang, M., He, Q., Jiang, Z., Zhu, W., Qiao, N., 2022. Global Dynamic Rainfall-Induced Landslide Susceptibility Mapping Using Machine Learning. Remote Sens. 14, 5795. https://doi.org/10.3390/rs14225795

https://doi.org/10.5194/egusphere-2026-458
Preprint. Discussion started: 4 February 2026

Liébault, F., Melun, G., Piton, G., Chapuis, M., Passy, P., Tacon, S., 2024. Channel change during catastrophic flood: Example of Storm Alex in the Vésubie and Roya valleys. Geomorphology 446, 109008. https://doi.org/10.1016/j.geomorph.2023.109008

Lionello, P., Malanotte-Rizzoli, P., Boscolo, R., 2006. Mediterranean climate variability.

Lombardo, L., Cama, M., Maerker, M., Rotigliano, E., 2014. A test of transferability for landslides susceptibility models under extreme climatic events: application to the Messina 2009 disaster. Nat. Hazards 74, 1951–1989. https://doi.org/10.1007/s11069-014-1285-2

Lombardo, L., Opitz, T., Ardizzone, F., Guzzetti, F., Huser, R., 2020. Space-time landslide predictive modelling. Earth-Sci. Rev. 209, 103318. https://doi.org/10.1016/j.earscirev.2020.103318

Lucas, T., 2023. Proposition d'une carte de susceptibilité glissement de terrain sur le département des Alpes-Maritimes (06) dans le cadre de la réalisation d'un système de vigilance (Mémoire de stage). Aix Marseille Université.

Marra, F., 2019. Rainfall thresholds for landslide occurrence: systematic underestimation using coarse temporal resolution data. Nat. Hazards 95, 883–890. https://doi.org/10.1007/s11069-018-3508-4

Melillo, M., Brunetti, M.T., Peruccacci, S., Gariano, S.L., Guzzetti, F., 2015. An algorithm for the objective reconstruction of rainfall events responsible for landslides. Landslides 12, 311–320. https://doi.org/10.1007/s10346-014-0471-3

Melillo, M., Brunetti, M.T., Peruccacci, S., Gariano, S.L., Roccati, A., Guzzetti, F., 2018. A tool for the automatic calculation of rainfall thresholds for landslide occurrence. Environ. Model. Softw. 105, 230–243. https://doi.org/10.1016/j.envsoft.2018.03.024

Montrasio, L., Valentino, R., 2008. A model for triggering mechanisms of shallow landslides. Nat. Hazards Earth Syst. Sci. 8, 1149–1159. https://doi.org/10.5194/nhess-8-1149-2008

Moreno, M., Lombardo, L., Crespi, A., Zellner, P.J., Mair, V., Pittore, M., van Westen, C., Steger, S., 2024. Space-time data-driven modeling of precipitation-induced shallow landslides in South Tyrol, Italy. Sci. Total Environ. 912, 169166. https://doi.org/10.1016/j.scitotenv.2023.169166

Ng, C.W.W., Yang, B., Liu, Z.Q., Kwan, J.S.H., Chen, L., 2021. Spatiotemporal modelling of rainfall-induced landslides using machine learning. Landslides 18, 2499–2514. https://doi.org/10.1007/s10346-021-01662-0

Nocentini, N., Rosi, A., Piciullo, L., Liu, Z., Segoni, S., Fanti, R., 2024. Regional-scale spatiotemporal landslide probability assessment through machine learning and potential applications for operational warning systems: a case study in Kvam (Norway). Landslides 21, 2369–2387. https://doi.org/10.1007/s10346-024-02287-9

Park, S., Kim, J., 2019. Landslide Susceptibility Mapping Based on Random Forest and Boosted Regression Tree Models, and a Comparison of Their Performance. Appl. Sci. 9, 942. https://doi.org/10.3390/app9050942

Peres, D.J., Cancelliere, A., 2021. Comparing methods for determining landslide early warning thresholds: potential use of non-triggering rainfall for locations with scarce landslide data availability. Landslides 18, 3135–3147. https://doi.org/10.1007/s10346-021-01704-7

https://doi.org/10.5194/egusphere-2026-458
Preprint. Discussion started: 4 February 2026

Peruccacci, S., Brunetti, M.T., Luciani, S., Vennari, C., Guzzetti, F., 2012. Lithological and seasonal control on rainfall thresholds for the possible initiation of landslides in central Italy. Geomorphology 139–140, 79–90. https://doi.org/10.1016/j.geomorph.2011.10.005

Pradhan, A.M.S., Kim, Y.T., 2016. Evaluation of a combined spatial multi-criteria evaluation model and deterministic model for landslide susceptibility mapping. CATENA 140, 125–139. https://doi.org/10.1016/j.catena.2016.01.022

Ran, Q., Hong, Y., Li, W., Gao, J., 2018. A modelling study of rainfall-induced shallow landslide mechanisms under different rainfall characteristics. J. Hydrol. 563, 790–801. https://doi.org/10.1016/j.jhydrol.2018.06.040

Rebora, N., Molini, L., Casella, E., Comellas, A., Fiori, E., Pignone, F., Siccardi, F., Silvestro, F., Tanelli, S., Parodi, A., 2013. Extreme Rainfall in the Mediterranean: What Can We Learn from Observations? J. Hydrometeorol. 14, 906–922. https://doi.org/10.1175/JHM-D-12-083.1

Reichenbach, P., Rossi, M., Malamud, B.D., Mihir, M., Guzzetti, F., 2018. A review of statistically-based landslide susceptibility models. Earth-Sci. Rev. 180, 60–91. https://doi.org/10.1016/j.earscirev.2018.03.001

Segoni, S., Piciullo, L., Gariano, S.L., 2018. A review of the recent literature on rainfall thresholds for landslide occurrence. Landslides 15, 1483–1501. https://doi.org/10.1007/s10346-018-0966-4

Shou, K.-J., Lin, J.-F., 2020. Evaluation of the extreme rainfall predictions and their impact on landslide susceptibility in a sub-catchment scale. Eng. Geol. 265, 105434. https://doi.org/10.1016/j.enggeo.2019.105434

Steger, S., Moreno, M., Crespi, A., Luigi Gariano, S., Teresa Brunetti, M., Melillo, M., Peruccacci, S., Marra, F., De Vugt, L., Zieher, T., Rutzinger, M., Mair, V., Pittore, M., 2024. Adopting the margin of stability for space–time landslide prediction – A data-driven approach for generating spatial dynamic thresholds. Geosci. Front. 15, 101822. https://doi.org/10.1016/j.gsf.2024.101822

Suleymanov, A., Richer-de-Forges, A.C., Saby, N.P.A., Arrouays, D., Martin, M.P., Bispo, A., 2024. National-scale digital soil mapping performances are related to covariates and sampling density: Lessons from France. Geoderma Reg. 37, e00801. https://doi.org/10.1016/j.geodrs.2024.e00801

Sun, D., Wen, H., Wang, D., Xu, J., 2020. A random forest model of landslide susceptibility mapping based on hyperparameter optimization using Bayes algorithm. Geomorphology 362, 107201. https://doi.org/10.1016/j.geomorph.2020.107201

Suradi, M., Fourie, A.B., Saynor, M.J., 2016. An experimental and numerical study of a landslide triggered by an extreme rainfall event in northern Australia. Landslides 13, 1125–1138. https://doi.org/10.1007/s10346-015-0606-1

Taalab, K., Cheng, T., Zhang, Y., 2018. Mapping landslide susceptibility and types using Random Forest. Big Earth Data 2, 159–178. https://doi.org/10.1080/20964471.2018.1472392

Terlien, M.T.J., 1998. The determination of statistical and deterministic hydrological landslide-triggering thresholds. Environ. Geol. 35, 124–130. https://doi.org/10.1007/s002540050299

Thiery, Y., Rault, C., Fressard, M., Ferradou, L., Kerverdo, R., Lafuerza, S., Bernardie, S., Marçot, N., Armand, L., 2025. Storm Alex and landslide-driven erosion in steep Mediterranean catchments. Journ. Aléas Gravitaires.

https://doi.org/10.5194/egusphere-2026-458
Preprint. Discussion started: 4 February 2026

Trigila, A., Iadanza, C., Esposito, C., Scarascia-Mugnozza, G., 2015. Comparison of Logistic Regression and Random Forests techniques for shallow landslide susceptibility assessment in Giampilieri (NE Sicily, Italy). Geomorphology, Geohazard Databases: Concepts, Development, Applications 249, 119–136. https://doi.org/10.1016/j.geomorph.2015.06.001

Tsai, T.-L., 2008. The influence of rainstorm pattern on shallow landslide. Environ. Geol. 53, 1563–1569. https://doi.org/10.1007/s00254-007-0767-x

Weiss, A., 2001. Topographic Position and Landforms Analysis.

Xu, C., Xu, X., Dai, F., Saraf, A.K., 2012. Comparison of different models for susceptibility mapping of earthquake triggered landslides related with the 2008 Wenchuan earthquake in China. Comput. Geosci. 46, 317–329. https://doi.org/10.1016/j.cageo.2012.01.002

Zevenbergen, L.W., Thorne, C.R., 1987. Quantitative analysis of land surface topography. Earth Surf. Process. Landf. 12, 47–56. https://doi.org/10.1002/esp.3290120107

Zhang, S., Li, L., Zhao, D., Ni, B., Qiang, Y., Zheng, Z., 2022. Stability and time-delay effect of rainfall-induced landslide considering air entrapment. Geosci. Lett. 9, 8. https://doi.org/10.1186/s40562-022-00216-z

Zhou et al., 2021. Landslide susceptibility mapping using hybrid random forest with GeoDetector and RFE for factor optimization.